SLAC-17
UC-28, Particle Accelerators
and High-Voltage Machines
UC-34, Physics
TID-4500

INVESTIGATIONS OF TRAVELING-WAVE SEPARATORS FOR THE STANFORD TWO-MILE LINEAR ACCELERATOR

August 1963

by

O. A. Altenmueller, R. R. Larsen and G. A. Loew

Technical Report
Prepared Under
Contract AT(04-3)-400
for the USAEC
San Francisco Operations Office

Printed in USA. Price $1.25. Available from the Office of Technical Services, Department of Commerce, Washington 25, D.C.

Acknowledgement

The authors wish to acknowledge the cooperation of several SLAC departments which contributed to this work, in particular the Fabrication Department which promptly fabricated the two experimental models, the Mark IV accelerator group which contributed to the installation and experiments, and George Jackson, who installed the extensive microwave circuitry.

Note: This paper was presented at the 1963 International Conference on High Energy Accelerators at Dubna, U.S.S.R., August 21-27, 1963.

TABLE OF CONTENTS

LIST OF FIGURES

I. INTRODUCTION

A. General Discussion

The idea of using rf fields to achieve mass separation of multi-bev particles has received considerable attention in the past few years. Prompted by W.K.H. Panofsky's proposal,[2] several laboratories have engaged in investigations of the subject. The first experimental attempt to deflect high-energy particles with microwave fields was made by P. R. Phillips [19] at Stanford. Programs to construct and use rf separators are presently underway at CERN (Geneva, Switzerland), Brookhaven National Laboratory (Upton, Long Island, New York), E.N.S. Orsay (Orsay, France) and the Stanford Linear Accelerator Center (Stanford, California).

Following a brief review of other approaches to the problem of mass separation, this paper will describe the investigations presently undertaken at Stanford to design and test traveling-wave separators for the two-mile linear accelerator. Attention will be focused on the separation of particles that are bunched at production.

The distinction between rf separators for bunched and unbunched beams is not a fundamental one; both cases make use of particle interaction with a transversely deflecting mode. However, they differ considerably in their experimental setups. Figure 1 illustrates an rf separator for unbunched beams. A continuous stream of both wanted (W) and unwanted (U) particles emerges from the target and is momentum analyzed. The first rf system or "modulator" indiscriminately deflects all particles at an angle determined by the entrance phase at the modulator. The beam transport system then refocuses the beam into the second rf system or "separator." The length of L is chosen so that the unwanted particles (U) have been shifted in phase by π* with respect to the wanted (W) particles. The phase of the separator

---

*The general relation giving the phase difference of two relativistic particles of the same momentum p and of rest energies W_{o1} and W_{o2} drifting over a distance L is

$$\tau = \frac{\omega L}{2c}\left(\frac{W_{o1}^2 - W_{o2}^2}{p^2c^2}\right)$$

where ω is the radial frequency and it has been assumed that

$$\frac{v}{c} \simeq 1 - \frac{W_o^2}{2p^2c^2}$$

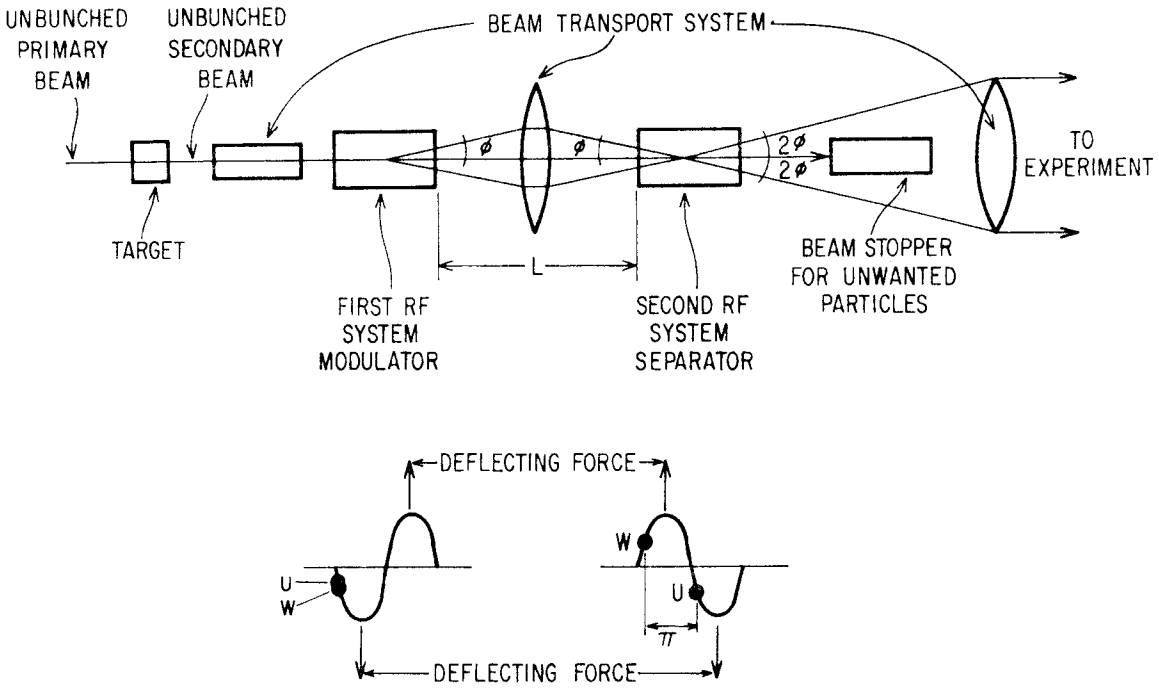

FIG. 1--Typical experimental layout of an rf separator for an unbunched beam. Wanted particles (W) and unwanted particles (U) are shown in their respective phases in the "modulator" and in the "separator." Notice π phase shift obtained between particles over distance L.

is then adjusted so that the original deflection of the U-particles is cancelled and the deflection of the W-particles is enhanced by a factor of two. The U-particles are eliminated by means of a beam stopper; the W-particles are transported into the experimental area. Since all particles that arrive at the modulator around the phase of zero deflecting field are collected by the beam stopper, this system will lose some wanted particles. All those particles that miss the beam stopper have, in principle, the same mass. Because of the low duty cycle (typically a few μsec pulse width) of the presently available high-power klystrons, this system can only be used for rapidly ejected beams.

Figure 2 shows an rf separator system for bunched beams in which no modulator is necessary. The bunched primary beam hits the target and produces a bunched secondary beam. The distance between the target and the rf separator is adjusted so that the U- and the W-particles slip with respect to each other by π. Hence, when they enter the separator they experience equal but opposite deflecting forces. The klystron powering the separator can be of the same type as those used for acceleration and can be locked to the trigger and drive systems of the accelerator. By adjusting the phase of the separator, the particles can be made to "ride the crest" of the deflecting wave, thus undergoing maximum separation.

B. RF Separators vs. DC Separators

At high energies, the reason for going to rf separators instead of simply extending dc devices is the following: The difference in momentum imparted to two particles traveling through the same dc deflecting field is simply proportional to the difference in their time-of-flight through the field. This difference is proportional to the inverse of the momentum squared. In an rf device the particles to be separated experience opposite transverse deflections and the difference in imparted momenta is proportional to the time-of-flight itself; for relativistic particles, this time-of-flight is momentum independent. The $(momentum)^{-2}$ ratio between dc and rf separators is the primary reason for resorting to rf devices in multi-bev particle separation. Given dc and rf devices of the same equivalent field strength, the dc device would have to fill the entire drift space provided for the rf device if it were to achieve the same separation as an rf structure one-half wavelength long. Clearly, the problems of field uniformity and stability over such distances are formidable. The necessity of providing long drift distances for rf devices in order to obtain the required phase slippage is no great disadvantage since the distances involved are comparable to the lengths of the beam transport systems which would be required.

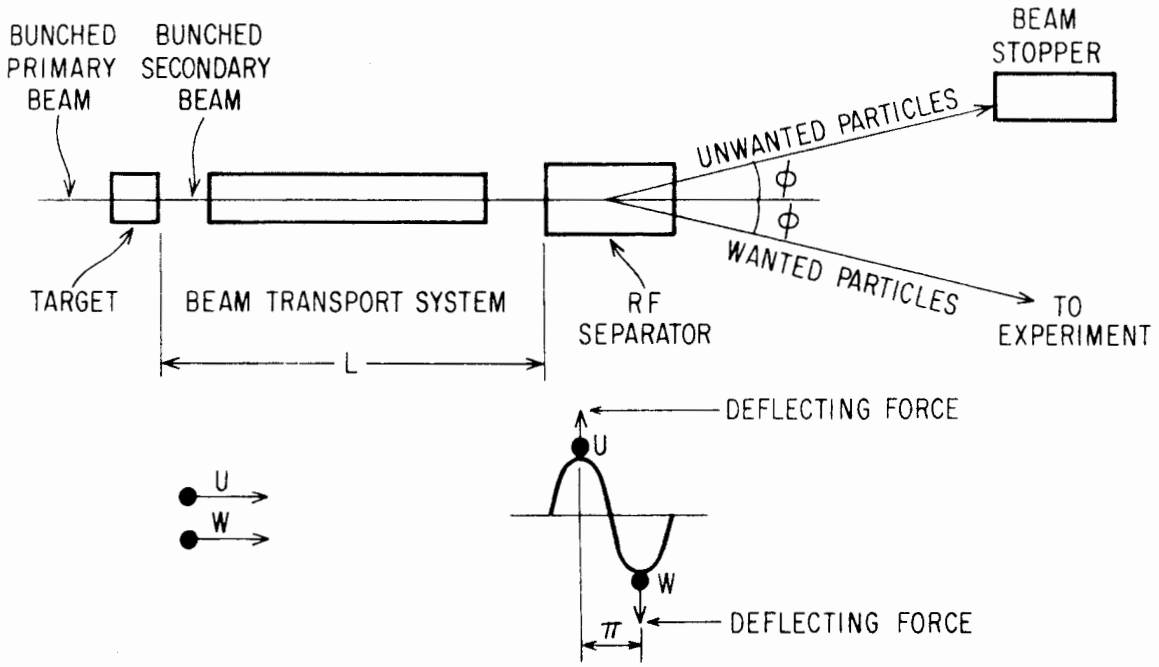

FIG. 2--Proposed experimental layout of an rf separator for a bunched beam. Wanted particles (W) and unwanted particles (U) are shifted in phase by π with respect to each other over distance L.

II. THEORY AND DESIGN OPTIMIZATION OF RF SEPARATORS

A. Traveling-Wave Versus Standing-Wave Separators

The theory and design of rf separators is similar to that of linear accelerators. Like linear accelerators, rf separators can be of the standing-wave or the traveling-wave type. In the standing-wave case, the structure is resonant and the fields are allowed to build up in time through multiple reflections before the particles are injected. The structure can consist of a single cavity (Phillips type) or of several cavities capped-off at the end.

Standing-wave separators have the following disadvantages:

(1) Only one-half of the power fed into the structure contributes to the useful deflection of particles. The other half of the power propagates in a direction opposite to the beam and does not assist in the deflection process. Hence, the relative efficiency of deflection is reduced as compared to the traveling-wave case.

(2) The fields in the standing-wave structure build up from zero to the steady-state value E_{ss} according to the expression

$$\frac{E}{E_{ss}} = 1 - e^{-\frac{\omega t}{2Q_L}} \qquad (1)$$

where $\omega = 2\pi f$ is the radial frequency, t is the time after start of build-up and Q_L is the loaded Q of the cavity. For maximum power transfer, $Q_L = Q_o/2$ where Q_o is the unloaded Q of the cavity. Hence, after a time $t_e = 2Q_L/\omega$, the fields will only have reached 63.2 percent of their final value. Assuming a value of $Q_o = 15{,}000$ and the standard Stanford frequency $f = 2856$ Mc/sec, $t_e = 0.837$ μsec. Particles injected during the build-up time will undergo deflections proportional to the field strength at the time of transit. Hence, unless injection is delayed for about $5t_e$, there will be a corresponding spread in deflection which is undesirable.

(3) The load impedance presented by the standing-wave separator also varies during the build-up period. At $t = 0$, the impedance is zero; i.e., the cavity appears as a short circuit. For $Q_o = 2Q_L$ and $\omega = \omega_o$ (the resonant frequency), the impedance can be shown to vary during the build-up period as

$$\frac{Z}{Z_o} = \frac{1 - \exp(-\omega t/2Q_L)}{1 + \exp(-\omega t/2Q_L)} \qquad (2)$$

Hence, for the same parameters as above and after a time t_e, the impedance will have reached only 46.2 percent of its final value, a build-up even

slower than for the fields. This change in impedance will cause the output from the rf source feeding the structure to vary during the build-up period, thereby adding to the deflection "spread." Unless an isolator or an attenuator is used to isolate the power source from the load, excessive electric gradients in the waveguides resulting from power reflections may cause damage to the power source. In addition, the isolator or the attenuator will introduce extra losses, thereby decreasing overall efficiency.

In the traveling-wave case, the rf fields propagate in only one direction along the structure; the energy travels at the group velocity v_g. After a time $t_f = \ell/v_g$ (the filling time) where ℓ is the length of the separator, the maximum field build-up is attained and the particles can be injected. The residual power at the end of the structure can be absorbed in an rf load, fed back by means of an external waveguide at the proper phase for greater field build-up, or fed into a subsequent rf structure. If the rf pulse length is not greater than twice the filling time, the wave can be allowed to reflect from the end of the structure without affecting the performance of the separator or the power source.

This paper will concern itself exclusively with traveling-wave separators of the simplest type, i.e., those in which the residual power is fed into an rf load. A brief discussion in the conclusion compares these results with those obtainable with resonant cavities.

B. Principle of Traveling-Wave RF Deflection

The principle of rf deflection has been studied by several authors (see List of References). This paper attempts to obtain explicitly those expressions which yield an optimum design in terms of physically measurable quantities.

Consider a structure of length ℓ through which an electromagnetic wave is transmitted, where E and B are the electric and magnetic fields, respectively. The transverse momentum gained by a particle of velocity v and charge q, injected parallel to the z axis, is given by

$$p_\perp = q/v \int_0^\ell \left[\vec{E}_\perp + (\vec{v} \times \vec{B})_\perp\right] dz \qquad (3)$$

In terms of the vector potential $\vec{A}$, we obtain

$$\vec{p}_\perp = \frac{q}{v}\int_0^\ell \left[-\frac{d}{dt}\vec{A}_\perp + \vec{\nabla}_\perp(\vec{v}\cdot\vec{A})\right]dz \tag{4}$$

$$= -\frac{q}{v}\left[\vec{A}_\perp(\ell) - \vec{A}_\perp(0)\right] + \frac{q}{v}\int_0^\ell \vec{\nabla}_\perp(\vec{v}\cdot\vec{A})\,dz \tag{5}$$

If the beginning and end of the structure consist of waveguides beyond cut-off, then the first term vanishes. Assuming that v remains constant in direction and magnitude, the second term becomes

$$\vec{p}_\perp = q\int_0^\ell \vec{\nabla}_\perp A_z\,dz \tag{6}$$

The fundamental problem in designing an rf separator is to find a structure which will support a mode for which $\nabla_\perp A_z$ does not vanish. Assuming at this point that such a structure can be found, and expressing A_z in terms of E_z,

$$p_\perp = -\frac{q}{\omega}\int_0^\ell \frac{\partial E_z}{\partial x}\,dz \tag{7}$$

In linear accelerators, it has been very useful to introduce the concept of shunt impedance defined as the ratio of the square of the energy gained per unit length to the power lost per unit length. In complete analogy, the transverse shunt impedance per unit length can be defined

$$r_T(x) = \frac{\left[(1/k)(\partial E_z/\partial x)\right]^2}{-(dP/dz)} \tag{8}$$

where k is the free-space wave number and P is the power flow in the structure. This quantity, which can in principle be measured experimentally, is one of the figures of merit of an rf separator. Expression (8) can be substituted in (7):

$$p_\perp = \frac{qk}{\omega}\int_0^\ell \sqrt{-r_T\frac{dP}{dz}}\,dz \tag{9}$$

Assuming a structure of modular construction, the power flow along the z-direction will be of the form:

$$P = P_o e^{-2Iz} \tag{10}$$

where P_o is the power input and $2I$ is the power attenuation. Hence, the total "transverse energy" gained by a particle riding the crest of the deflecting wave over the length ℓ becomes:

$$p_\perp c = q \int_0^\ell \sqrt{2 I r_T P_o}\, e^{-Iz}\, dz \tag{11}$$

or

$$p_\perp c = q\sqrt{2I\ell}\left(\frac{1 - e^{-I\ell}}{I\ell}\right)\sqrt{P_o \ell r_T} \tag{12}$$

The "transverse energy" can be maximized by proper choice of the parameters r_T, I and ℓ. r_T is a function of the structure configuration and the chosen mode.

C. The Deflecting Mode and Its Shunt Impedance

H. Hahn[34,35,36,45,46] of Brookhaven National Laboratory and Y. Garault[30-33] of Orsay, France have made extensive analytical studies of deflecting modes in iris-loaded cylindrical waveguides. Hahn's analysis is carried out in terms of what he calls hybrid modes (HM and HE); it avoids the difficulties incurred in the analysis involving the usual TM and TE modes for phase velocities $v_p = c$.*

By Fourier-analyzing the fields in an iris-loaded structure, Hahn and Garault obtain the following first order solution for the lowest order deflecting mode at $v_p = c$:

$$E_z = E_o\, kr \cos\theta \tag{13}$$

$$E_r = E_o\left[(kr/2)^2 + (ka/2)^2\right]\cos\theta \tag{14}$$

$$E_\theta = E_o\left[(kr/2)^2 - (ka/2)^2\right]\sin\theta \tag{15}$$

---

*B. Montague, CERN, private communication.

$$Z_o H_z = - E_o \, kr \sin \theta \tag{16}$$

$$Z_o H_r = - E_o \left[(kr/2)^2 - (ka/2)^2 + 1 \right] \sin \theta \tag{17}$$

$$Z_o H_\theta = E_o \left[(kr/2)^2 + (ka/2)^2 - 1 \right] \cos \theta \tag{18}$$

where k is the free-space wave-number and a is the radius of the iris aperture (see Fig. 3a). From the Lorentz force on a particle of charge q, one obtains for the forces in rectangular coordinates

$$F_y = 0 \tag{19}$$

$$F_x = qE_o \tag{20}$$

Hence, the equivalent deflecting field is uniform in magnitude and direction over the aperture. This property is desirable since it implies that one can expect an aberration-free deflection from this mode. Integrating the Poynting vector over the aperture, one obtains for the power in the z direction:

$$P_z = \pi a^2 \, E_o^2 / Z_o \; 1/2 \; (ka/2)^2 \left[4/3 \; (ka/2)^2 - 1 \right] \tag{21}$$

From this expression one can estimate the deflecting field per unit power input. One observes that this deflecting mode is a forward or a backward-wave mode depending on whether $ka > \sqrt{3}$ or $ka < \sqrt{3}$. For 2856 Mc/sec, the cross-over value of a is 2.9 cm.

Combining expressions (8) and (21), it is possible to obtain a theoretical expression for the shunt impedance

$$r_T = \frac{Z_o}{I \pi a^2 \, (ka/2)^2 \left[\frac{4}{3} \, (ka/2)^2 - 1 \right]} \tag{22}$$

It is seen that r_T is a function of the cavity dimensions and of I, the attenuation constant. Since

$$I = \frac{\omega}{2 v_g Q} \tag{23}$$

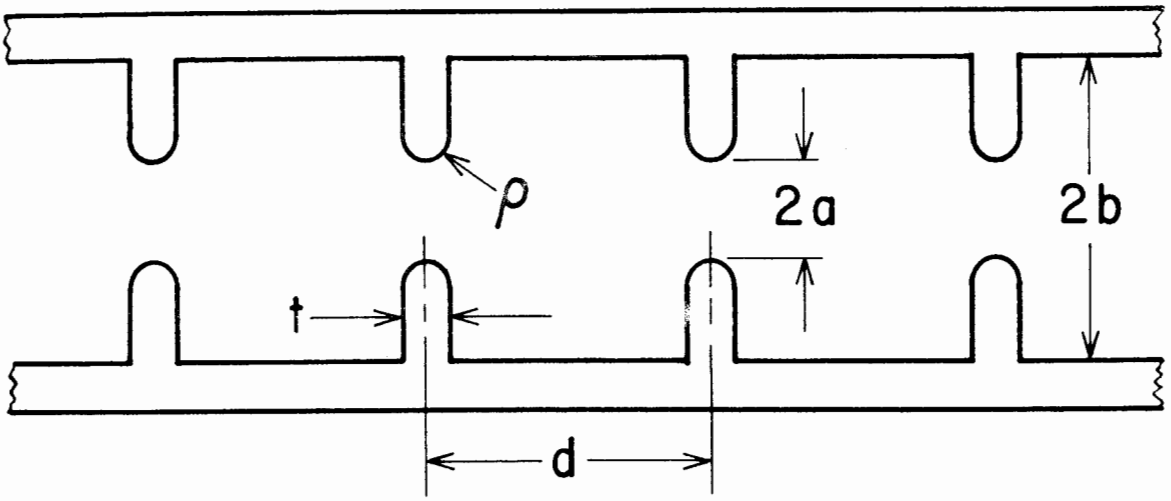

FIG. 3(a)--Schematic drawing of disk-loaded waveguide: modular dimensions of cavities.

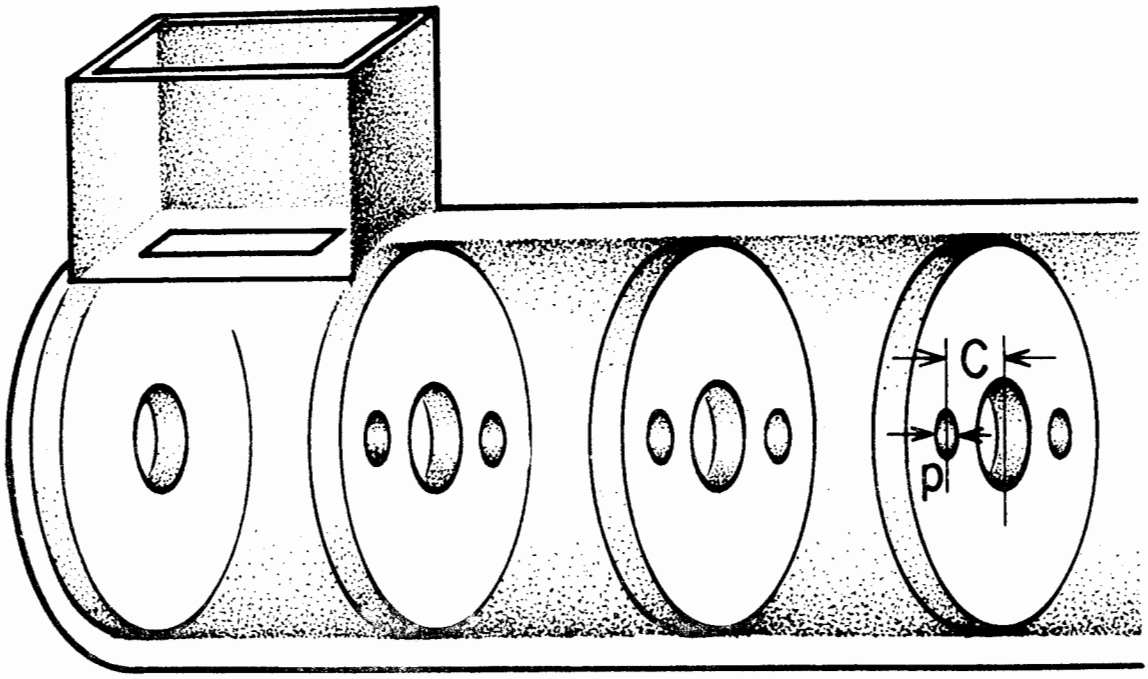

FIG. 3(b)--Schematic drawing of disk-loaded waveguide: disks with suppressor holes.

expression (22) can be rewritten as

$$\frac{r_T}{Q} = \frac{2Z_o v_g}{\omega\pi a^2 (ka/2)^2 \left[\frac{4}{3}(ka/2)^2 - 1\right]} \tag{24}$$

Unfortunately, we have no closed expression at this time for v_g; therefore, the quantity r_T/Q, which is purely dependent on the geometry of the structure and not on the losses, cannot be calculated. However, it will be shown in Section III. A how an approximate value of r_T/Q can be obtained experimentally.

Figure 4 shows the various ω-β diagrams obtainable for the HEM_{11} mode when the structure is a forward, a backward, or a mixed wave. The Brookhaven group has chosen to use a backward-wave mode at a phase shift per cavity of $\pi/2$. SLAC is investigating the same type of mode using the $2\pi/3$ point. CERN, on the other hand, has chosen to use a mixed-wave mode at the $\pi/2$ point. A possible disadvantage of the latter structure is that the diagram is double-valued so that two waves can be launched into the structure for a given frequency, which decreases the energy available for synchronous deflection. It is not yet known which of these structures is optimum in terms of shunt impedance.

D. Choice of the Attenuation Parameter $I\ell$

The normalized "transverse energy" is plotted in Fig. 5 for a given length of structure ℓ. Equation (11) has its maximum at

$$I\ell = 1.26 \tag{25}$$

corresponding to a maximum obtainable "transverse energy"

$$(p_\perp c)_{max} = 0.903\, q\sqrt{P_o r_T \ell} \tag{26}$$

It is seen that the maximum "transverse energy" has a broad maximum and that the choice of $I\ell$ can be compromised if choosing a value other than $I\ell = 1.26$ presents other advantages. It is also seen that this method of feeding the separator is inherently quite efficient since it provides an energy 90 percent as high as would be obtained by feeding each cavity independently.

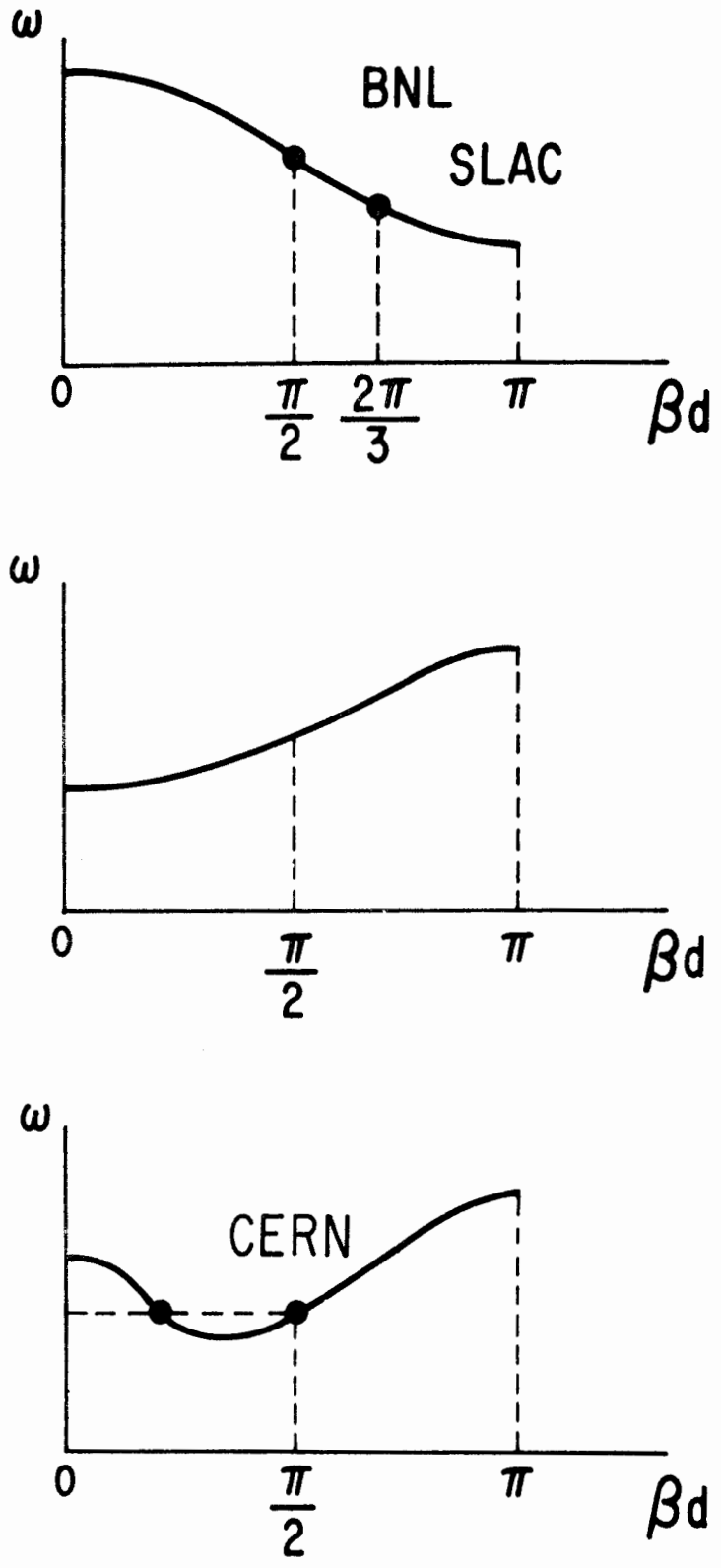

FIG. 4--Sketches of possible ω-β diagrams encountered in structures using HEM_{11} mode.

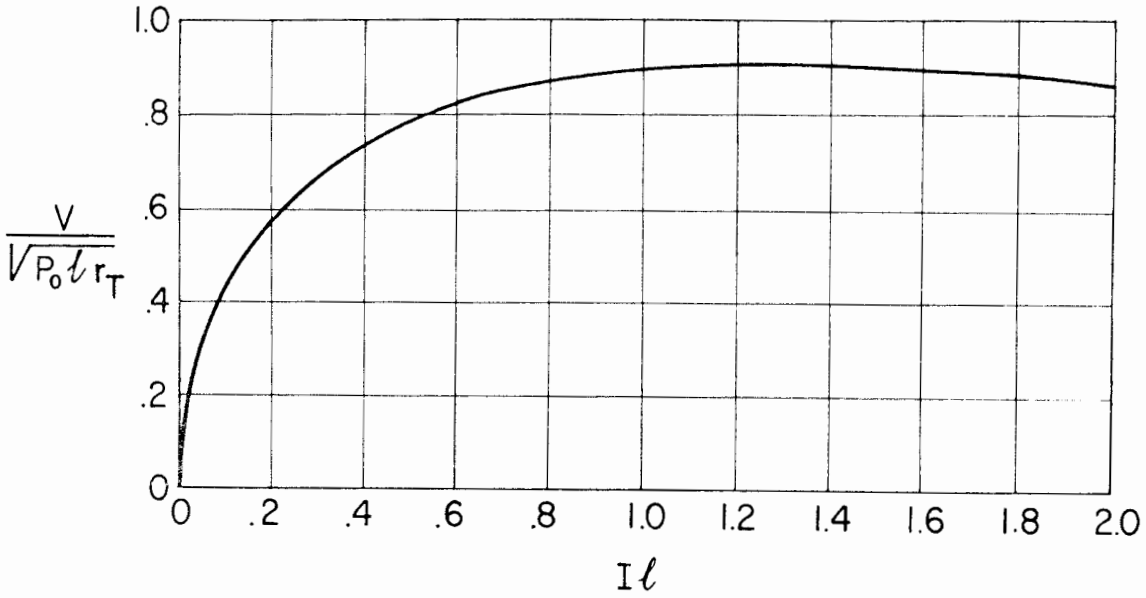

FIG. 5--Normalized deflection energy as a function of attenuation parameter $I\ell$. Notice maximum deflection occurs for $I\ell = 1.26$.

Another parameter which enters into the design of the rf separator is the filling time $t_f = \ell/v_g$. From Eq. (23)

$$t_f = \frac{2Q}{\omega} I\ell \tag{27}$$

Hence, if the separator klystron has the same pulse length as the accelerator klystrons, it is advantageous to choose a value of $I\ell$ which makes t_f no longer than the filling time for the accelerator sections. For a given frequency and a given quality factor Q, the desired value of I is obtained by adjustment of the dimensions indicated in Figs. 3a. and 3b.

E. Choice of Separator Length

The choice of separator length ℓ is guided by three factors: deflection efficiency, electrical breakdown, and acceptance.

Efficiency would dictate the choice of an infinite length because, as has been shown by R. B. Neal[4] for linear accelerators, 39 percent more deflecting energy can be obtained than with the finite optimized design using $I\ell = 1.26$.

Electrical breakdown limits the maximum allowable field strength in the structure. From common experience, this maximum is of the order of 200 kv/cm.

Assuming the choice of $I\ell = 1.26$, the longer the structure, the smaller I and the smaller the energy stored per unit length. Hence, a longer length permits a higher input power before the breakdown limit is attained.

It is also possible to reduce the field gradient for a given input power by designing a constant gradient structure.[28] In such a structure, the ratio of peak-to-average axial electric field strength is unity, while in the usual uniform (constant impedance) structure it can be as high as 1.76 for $I\ell = 1.26$. The constant gradient structure could produce a deflection 1.76 times as large as the optimized constant impedance structure when both are operating at the breakdown limit. In practice, such a constant gradient would be obtained by tapering the modular dimensions of the structure. For example, in the backward-wave structure proposed by Stanford, one would keep the energy density constant by decreasing the iris aperture in the direction of the longitudinal motion of the beam.

The utility of rf separators at multi-bev energies rests on their ability to transmit fluxes of sufficient intensity for experimental needs. Figure 6

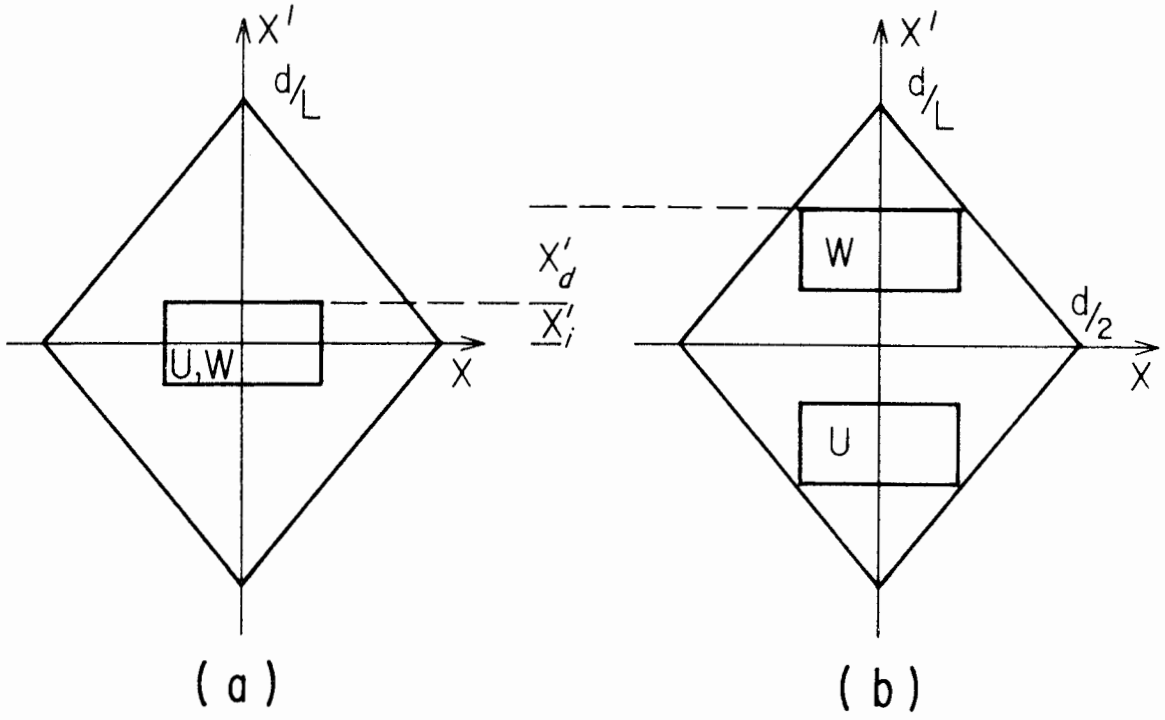

FIG. 6--Phase space area of beam in deflecting plane within boundaries of separator:
a. Before deflection
b. After deflection

illustrates the phase space of the beam (in the plane of separation) inscribed within the boundaries of the separator. The phase area is approximated by rectangles to facilitate the calculation of the acceptance. It is assumed that (1) the deflection is lumped at the center of the structure and (2) the emerging beam just grazes the separator. The following quantities are defined:

x, x' = linear and angular displacements in deflecting plane

y, y' = linear and angular displacements in non-deflecting plane

d_s = separator diameter (meters)

ℓ = separator length (meters)

E = equivalent deflecting field (mv/meter)

p = beam momentum (Mev/c)

x'_d = angle of deflection

α = E/pc (meter^{-1})

η = x'_d / x'_i where x'_i is the incident angular spread (i.e., $\eta = 1$ corresponds to the "just separated" situation).

The phase area incident in the deflecting plane is

$$a_i = 4x_i x'_i \tag{28}$$

Considering the geometry in Fig. 6 and using the above definitions this becomes

$$a_i = \frac{2\alpha}{\eta} \ell \left[d_s - \alpha \ell^2 (1 + 1/\eta) \right] \tag{29}$$

where

$$x'_d = \alpha \ell$$

The essential point is that one can only accept an incident angular spread that is less than the angular separation achieved. For $\ell = 0$ there is no deflection and hence $x'_i = 0$. For very large ℓ, the beam would be deflected into the separator walls. The acceptance can be optimized as a

function of ℓ, as

$$a_i = \frac{4}{3} d_s \sqrt{\frac{\alpha d_s}{3\eta(\eta + 1)}} \tag{30}$$

and

$$\ell_o = \sqrt{\frac{d_s \eta}{3\alpha(\eta + 1)}} \tag{31}$$

In the non-deflecting plane the acceptance for a given ℓ is maximum when

$$y_i' = d_s/2\ell \tag{32}$$

leading to an acceptance of

$$d_s^2/2\ell \tag{33}$$

If one optimized the net acceptance (product of deflecting and non-deflecting acceptance) one would be led to the unrealistic condition that $\ell = 0$. Taking into consideration the circular factors, one has for the maximum net acceptance

$$A_i = (\pi^2/24)(\alpha/\eta) d_s^3 = (\pi^2/24)(E/pc)(d_s^3/\eta) \tag{34}$$

This is composed of

$$\begin{aligned} x_i &= \frac{1}{3} d_s \\ x_i' &= \frac{\alpha}{\eta} \ell_o \\ y_i &= \frac{1}{4} d \\ y_i' &= \frac{d_s}{2\ell_o} \end{aligned} \tag{35}$$

For $E = 8$ mv/m, $d_s = 5$ cm, $\eta = 1$ and pc in Bev,

$$A_i = (40/pc) \times 10^{-4} \text{ ster - cm}^2 \tag{36}$$

and

$$\ell_o = \sqrt{pc} \text{ meters}$$

$$x'_d = 8/\sqrt{pc} \text{ milliradians}$$

In the energy region of 10-15 Bev, one would want a ℓ_o of three to four meters which would produce deflections of ≈ 2 milliradians. Although it is doubtful that one would be able to use the entire optimized acceptance because of the limitations of the beam transport system,[48] the acceptance of the rf structure is considerably greater than that of a dc separator.[38]

Assuming a length of 3 meters for a 10 Bev beam as a reasonable compromise between these three criteria, it is seen that for $I\ell = 1.26$, $I = 0.42 \text{ (meter)}^{-1}$. From Eq. 23 and for a Q of 10,000, one obtains $v_g/c = 0.0071$. This will yield an optimum design assuming that r_T/Q and Q are slowly varying functions which do not change rapidly with $2a$.

F. Choice of Frequency

In the case of separators to be used in connection with linear accelerators, the choice of operating frequency is not free. At Stanford this frequency is 2856 Mc/sec, corresponding to a free space wavelength of 10.5 cm. At the present time, the arguments for choosing such a frequency for the accelerator[28] are equally valid for the separator.

III. COLD TESTS AND FABRICATION OF RF STRUCTURE

A. Cold Tests

Two experimental models were designed and fabricated for testing on the Stanford Mark IV accelerator. Neither one was optimized in terms of the parameter $I\ell$ since the length of the separator to be used on the two-mile machine will be much greater than that of the models. Model I is a conventional circularly symmetrical disk-loaded waveguide as shown in Fig. 3a. Model II uses so-called "suppressor holes" as shown in Fig. 3b to prevent rotation of the deflecting plane caused by possible non-uniformities of the structure. Although it was not anticipated that there would be any rotation in a structure as short as the model, it was advisable to determine if the suppressors had any adverse effects on the deflection efficiency.

These empirical designs were obtained by means of conventional microwave techniques[5,28] using stacks of cylinders and disks. Table I outlines the physical dimensions and cold-test results. The cold-test frequency was adjusted to yield an operating frequency compatible with the operating frequency of the Mark IV accelerator.

Figure 7 shows the electric field configuration of the deflecting mode at $2\pi/3$ obtained by means of a sapphire bead probe in a Model I type test cell. Figure 8 gives the result of an electric field perturbation measurement along the transverse direction in the middle test cavity. Figure 9 gives a similar plot for a perturbation along the z-direction, close to the disk edge and along the diameter of maximum field. Notice that these frequency perturbation measurements yield the square of the field intensity.

An attempt was also made to measure the transverse shunt impedance by a perturbation technique. The method used to measure the longitudinal shunt impedance[28] cannot be applied directly. However, an approximate measurement can be made by measuring the frequency perturbations caused by an axial dielectric rod and bead at successive intervals x and $x + \Delta x$ from 0 to a along the diameter of maximum gradient. The rod measurement gives the total longitudinal shunt impedances divided by Q, $r_L(x)/Q$ and $r_L(x + \Delta x)/Q$. The bead measurement gives the relative space harmonic amplitudes

$$\frac{a_o^2(x)}{\sum_{-\infty}^{+\infty} a_n^2(x)} \quad \text{and} \quad \frac{a_o^2(x + \Delta x)}{\sum_{-\infty}^{+\infty} a_n^2(x + \Delta x)} \tag{36}$$

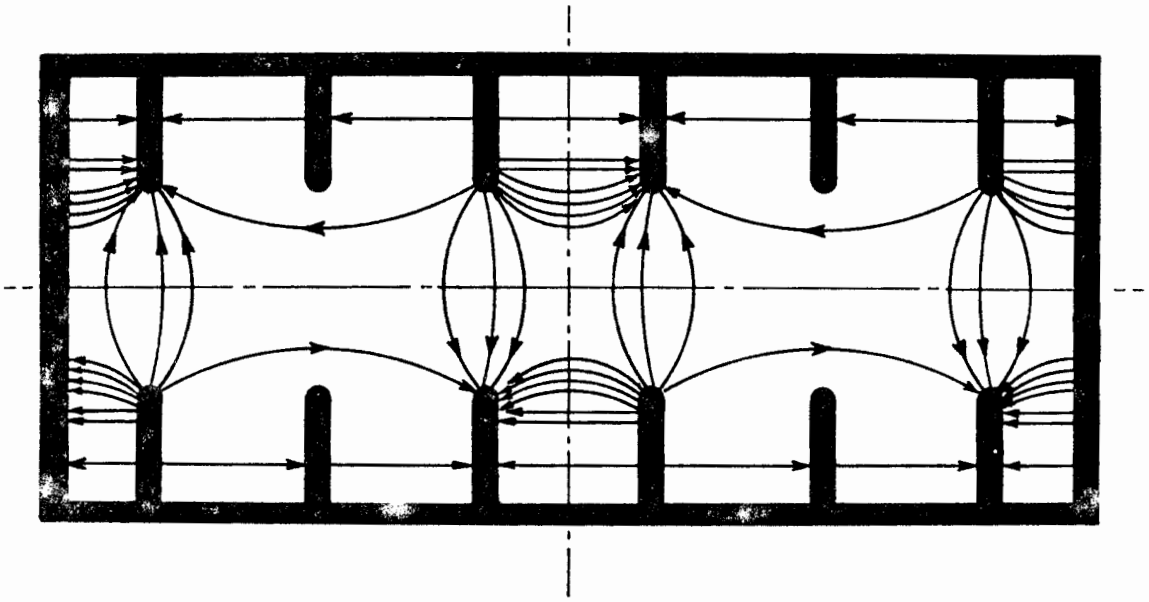

FIG. 7--"TM_{11}-like" or HEM_{11} electric field configuration in rf separator test-cell for $2\pi/3$ phase shift cavity.

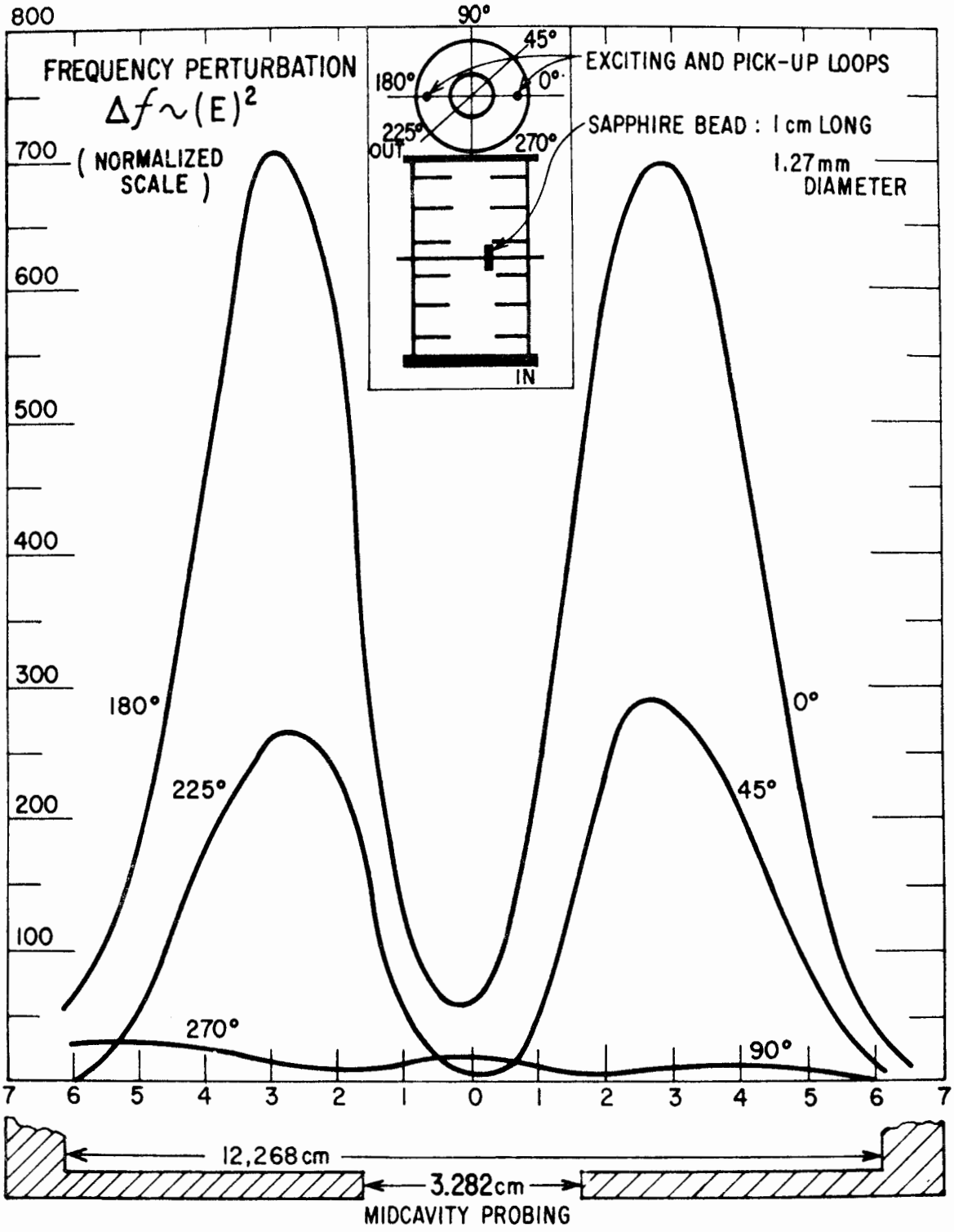

FIG. 8--Square of electric field intensity in mid-cavity of test cell as a function of radial and angular position (no suppressor holes).

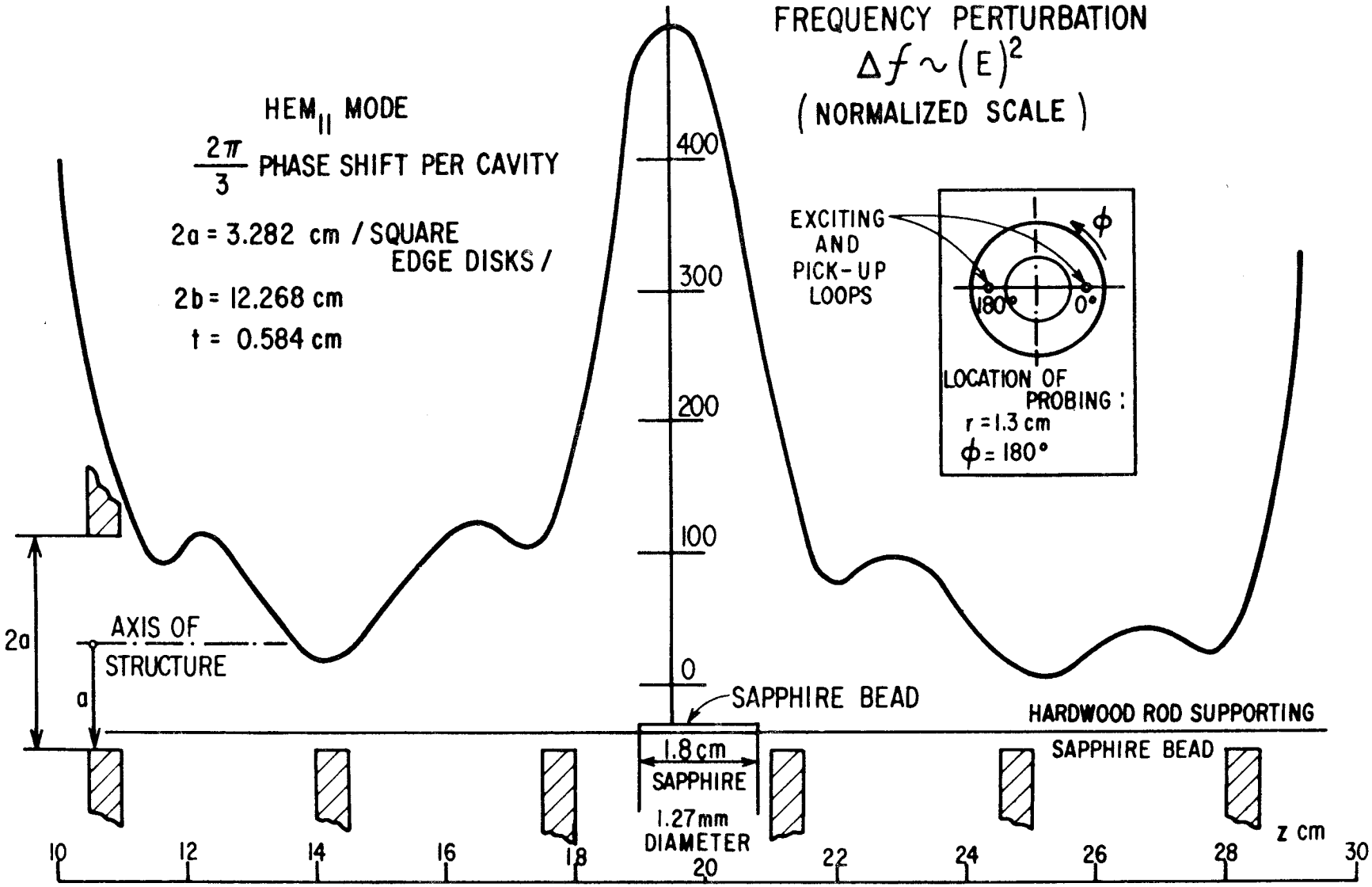

FIG. 9--Probing along z-direction close to disk edge. Square of electric field intensity as a function of z in test-cell with bead drawn close to disk edge ($\varphi = 180°$), no suppressor holes.

TABLE I

PHYSICAL DIMENSIONS AND COLD-TEST RESULTS FOR
RF SEPARATORS MODELS I AND II

Designation	Symbol	Model I	Model II
Length in cavities	ℓ	13 cavities and 2 couplers	13 cavities and 2 couplers
Periodic length	d	3.5 cm	3.5 cm
Phase shift per cavity		$2\pi/3$	$2\pi/3$
Inside cavity diameter	2b	11.8542 cm	11.7894 cm
Iris diameter	2a	4.064 cm	4.064 cm
Iris aperture radius	ρ	0.3086 cm	0.3086 cm
Disk thickness	t	0.584 cm	0.584 cm
Suppressor hole diameter	p		1.905 cm
Suppressor hole radial distance	c		3.620 cm
Inside coupler diameter	$2b_{CPL}$	11.659 cm	11.659 cm
Terminal cut-off hole diameter		3.3 cm	3.6 cm
Thickness of cut-off disks		4.762 cm	3.8 cm
Cold test frequency at 78°F and 42% relative humidity	f	2857.680 Mc/sec	2857.680 Mc/sec
Quality factor	Q	10700	9030
Relative group velocity	v_g/c	- 0.0311	- 0.0296
Attenuation	$I\ell$	0.047 nepers	0.058 nepers

The transverse shunt impedance divided by Q as defined by Eq. 8 can be given by

$$\frac{r_T\left[x + (\Delta x/2)\right]}{Q} = \left\{ \frac{1}{k} \frac{\left[\frac{a_o^2(x+\Delta x)}{\Sigma a_n^2(x+\Delta x)} \frac{r_L(x+\Delta x)}{Q}\right]^{\frac{1}{2}} - \left[\frac{a_o^2(x)}{\Sigma a_n^2(x)} \frac{r_L(x)}{Q}\right]^{\frac{1}{2}}}{\Delta x} \right\}^2 \tag{37}$$

The space harmonic measurement using the bead perturbation is a difficult one. Furthermore, the technique suffers from inaccuracies because the electric field is not everywhere parallel to the long side of the bead or the rod. An error of the order of 30 percent was found as compared with the shunt impedance derived from deflection experiments (Eq. 38).

Figure 10 gives the respective Brillouin or ω-β diagrams for structures very close in dimensions to Models I and II. It is important to notice how the 90° rotation of the axis of the suppressor holes with respect to the existing probes causes the ω-β diagrams to be separated. Hence, by aligning the suppressor holes at 90° with the couplers as shown in Fig. 3b, mode rotation should be entirely prevented.

B. Fabrication of Models I and II

Figures 11 and 12 respectively show a sketch and a photograph of the final structure. Both structures were built by brazing stacks of machined OFHC copper cylinders and disks. Referring to Figs. 3a and 3b, the following machining tolerances were observed:

2b	±0.0025 cm
2a	±0.0005 cm
d	±0.00075 cm
t	±0.0005 cm
ρ	±0.0012 cm
p	±0.0012 cm
c	±0.0012 cm

The brazing operation was carried out in four steps. First, the coupler cavities were furnace brazed. Their matching irises were then machined and checked for a rough match. Subsequently, two half stacks of six and seven

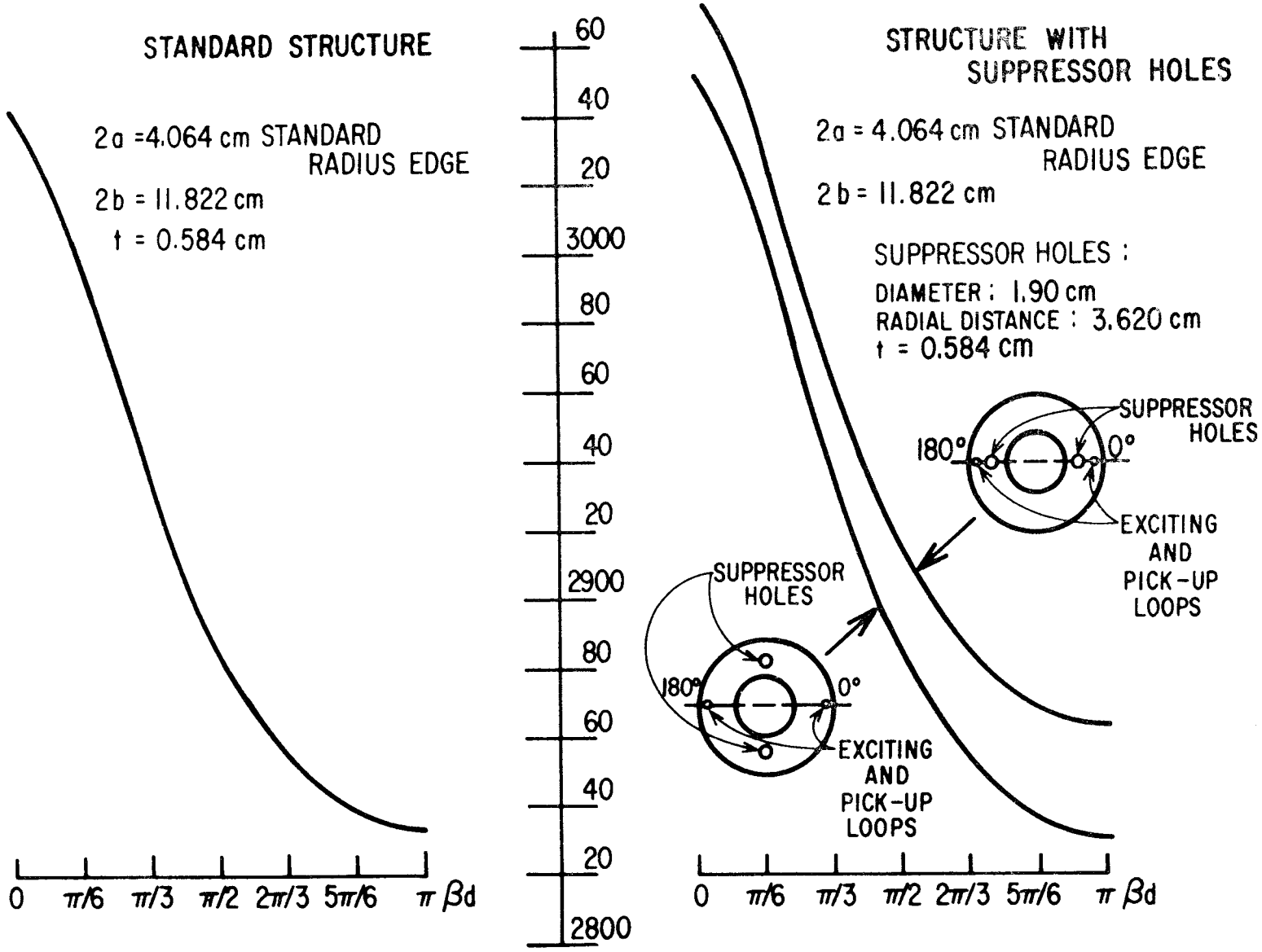

FIG. 10--ω-β diagrams for two rf separator designs.
a. Standard structure
b. Structure with suppressor holes

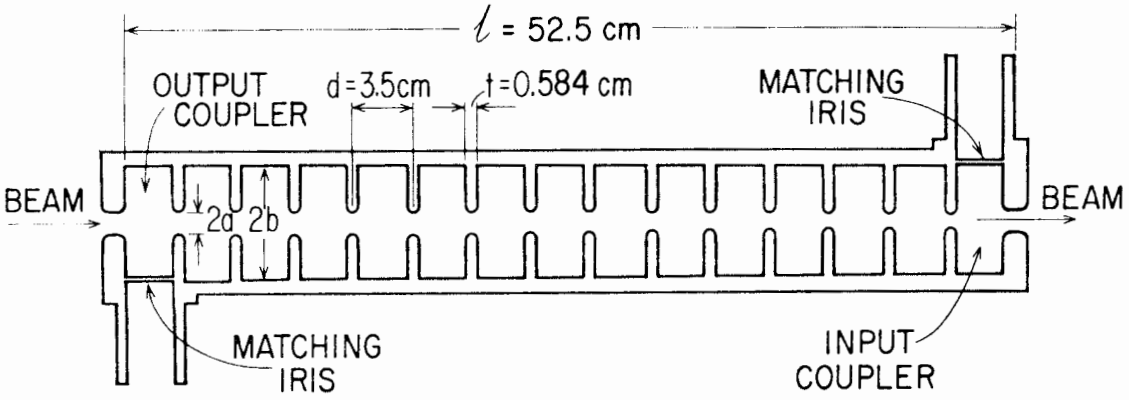

FIG. 11--Sketch of rf separator model with input and output couplers.

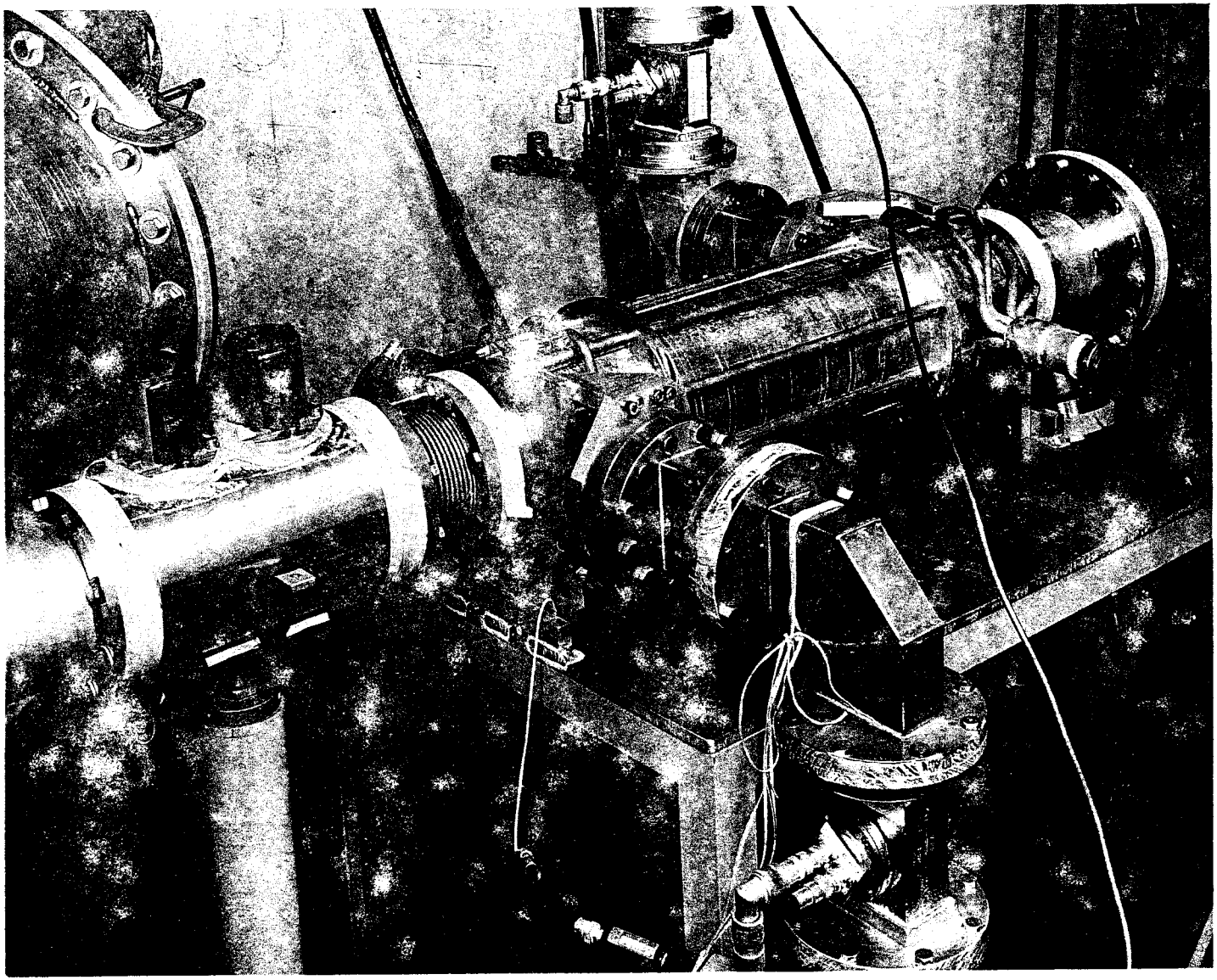

FIG. 12--RF separator: model showing input and output waveguides and water cooling pipes.

cavities respectively were brazed to the couplers. Both these operations were done with Nicoro at 1030°C. Next, the rectangular waveguide transitions were brazed onto the couplers using 50% copper-50% gold at 970°C. The last braze to join the two half-stacks was done using CuSil at 780°C. The vacuum flanges were heliarced, and the water cooling pipes were soft-soldered onto the wall of the structure. For the second separator, stainless steel mandrels were used to align the suppressor holes.

C. Matching of the Structures

After fabrication, both structures were submitted to a series of rf cold tests. These tests resemble closely those used to match and tune linear accelerator structures[5,28] and will not be described here. Machining and assembling tolerances were such that all cavity phase shifts came within $\pm 5^{\circ}$ of 120°, and no individual cavity tuning was deemed necessary. The coupling irises were matched using the nodal shift technique, both with a detuning plunger (1.27 cm in diameter) inserted into the structure and a sliding short in the output waveguide. Contrary to expectations, plungers of larger diameters did not give satisfactory results.

When performing the nodal shift technique, it is important to bear in mind that both structures are of the backward-wave type. This property causes the motion of the null in the slotted line as a function of the detuning plunger position to take place in the direction opposite to that obtained with a forward-wave structure. Furthermore, an increase in frequency here decreases the phase shift per cavity, whereas in a forward-wave structure an increase in frequency increases the phase shift per cavity.

The final VSWR into and out of the structures, including two ceramic vacuum windows, was of the order of 1.1:1.0. Notice that the input and output couplers have opposite orientations. This was done to cancel any possible spurious deflection caused by the field asymmetry due to the iris opening.

IV. PERFORMANCE OF RF SEPARATOR MODELS

A. General Description of Experiment

Before expending money and time on the design and construction of large high-power separators, it was considered advisable to demonstrate experimentally the

feasibility of traveling-wave separators. Several experiments were performed to measure directly the deflection capability of the structures described in Section III.

A schematic of the experimental arrangement is shown in Fig. 13. The electron beam of the 100-Mev Stanford Mark IV linear accelerator was momentum analyzed and transmitted through the separator. As the magnitude and phase of the microwave fields in the separator were varied, the motion of the electron beam in the horizontal plane was observed on a ZnS screen mounted on the end of a 2-meter evacuated drift tube that followed the separator.

B. Microwave System

Referring again to Fig. 13, it can be seen how the overall layout of the Mark IV accelerator was used to power the rf separator and to test its deflection properties. Of the two klystrons available in the machine, a fraction of the output of the second tube was coupled off the main waveguide feeding the second accelerator section by means of a 7 db directional coupler (see Fig. 14). Independent power level and phase control were achieved by means of a manually driven attenuator (left of Fig. 14) and a motor driven trombone-type phase shifter (right of Fig. 14). Following the phase shifter, a high power switch enabled one to transmit the microwave power to the rf separator or to dissipate it into a matched high power load. Input and output rf power levels were monitored by means of directional couplers (52.8 db and 52.4 db) and standard bolometer power bridges. The output of the separator looked into a pressurized matched load. The complete rf assembly from the 7 db directional coupler to the separator was isolated from the accelerator vacuum system by means of two ceramic windows, and it was pressurized to 30 pounds of freon.

C. Electron Beam

The energy of the electron beams was of the order of 30 to 50 Mev ($\pm \approx 1\%$). This energy region permitted easily observable deflections and stable operation of the accelerator. For a given power output of the klystrons, the beam transmitted through the momentum slits (monitored by the Faraday cup and the ZnS screen) was optimized by varying the current in the wedge-shaped analyzing magnet (30° bend) [see Fig. 15]. An analyzed beam current of 1 mμamp was easily observed on the screen (see Fig. 16).

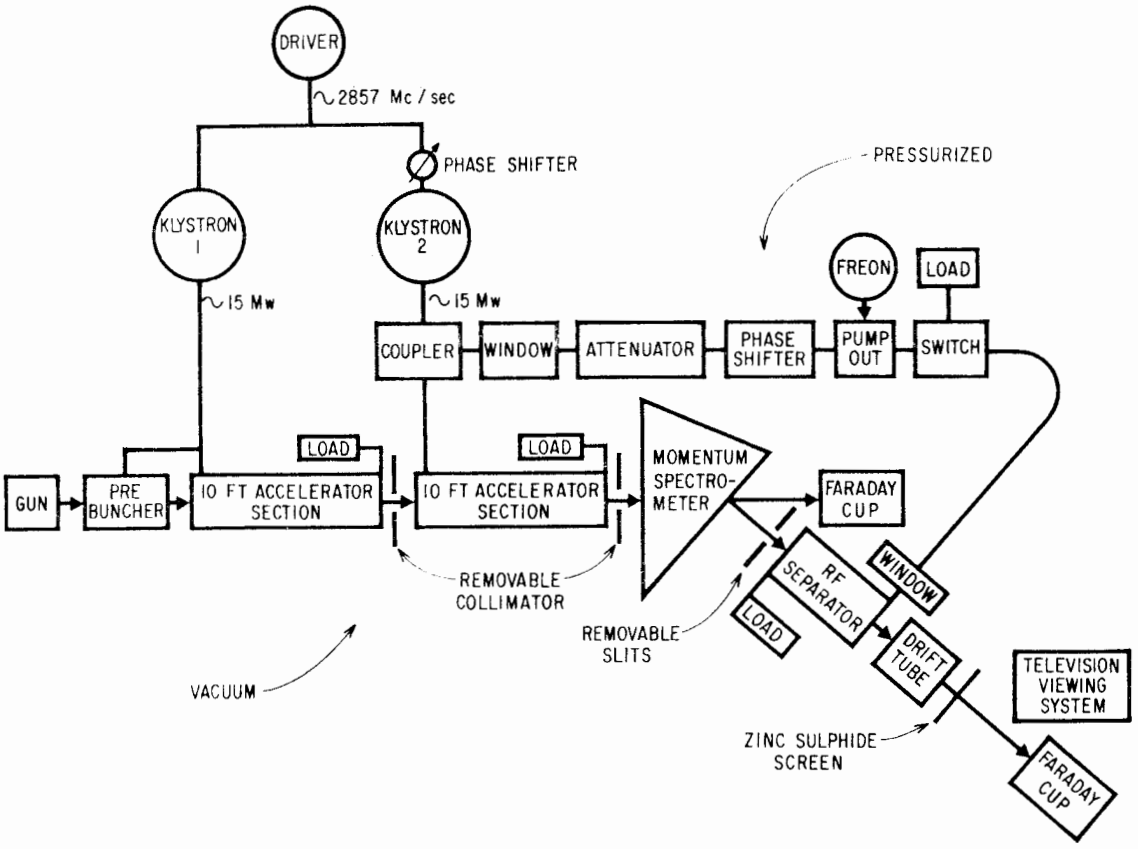

FIG. 13--Mark IV layout showing two accelerator sections with respective klystrons and rf separator with microwave circuitry.

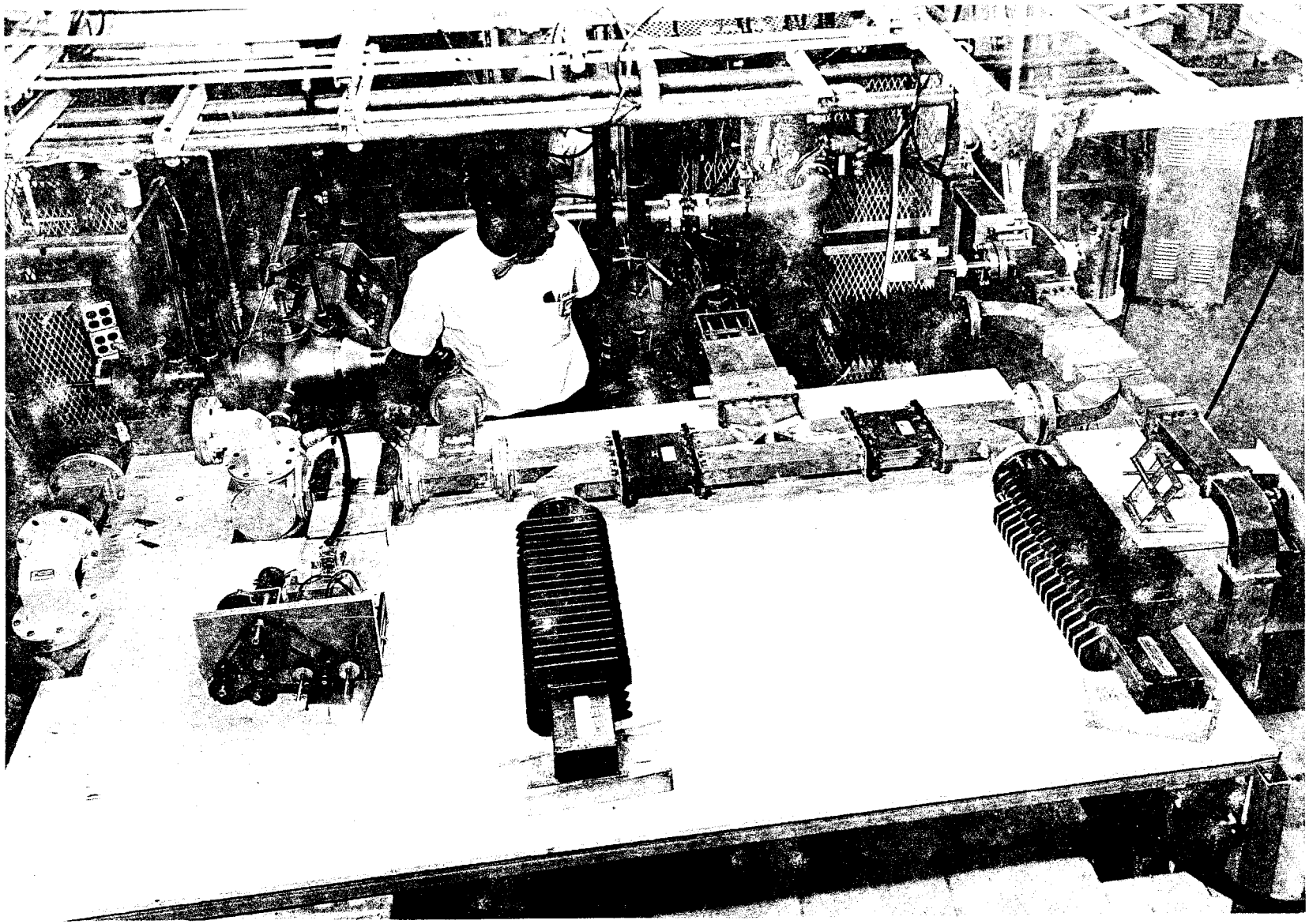

FIG. 14--Microwave circuitry for rf separator showing directional coupler, attenuator, pumpout, phase shifter and switch.

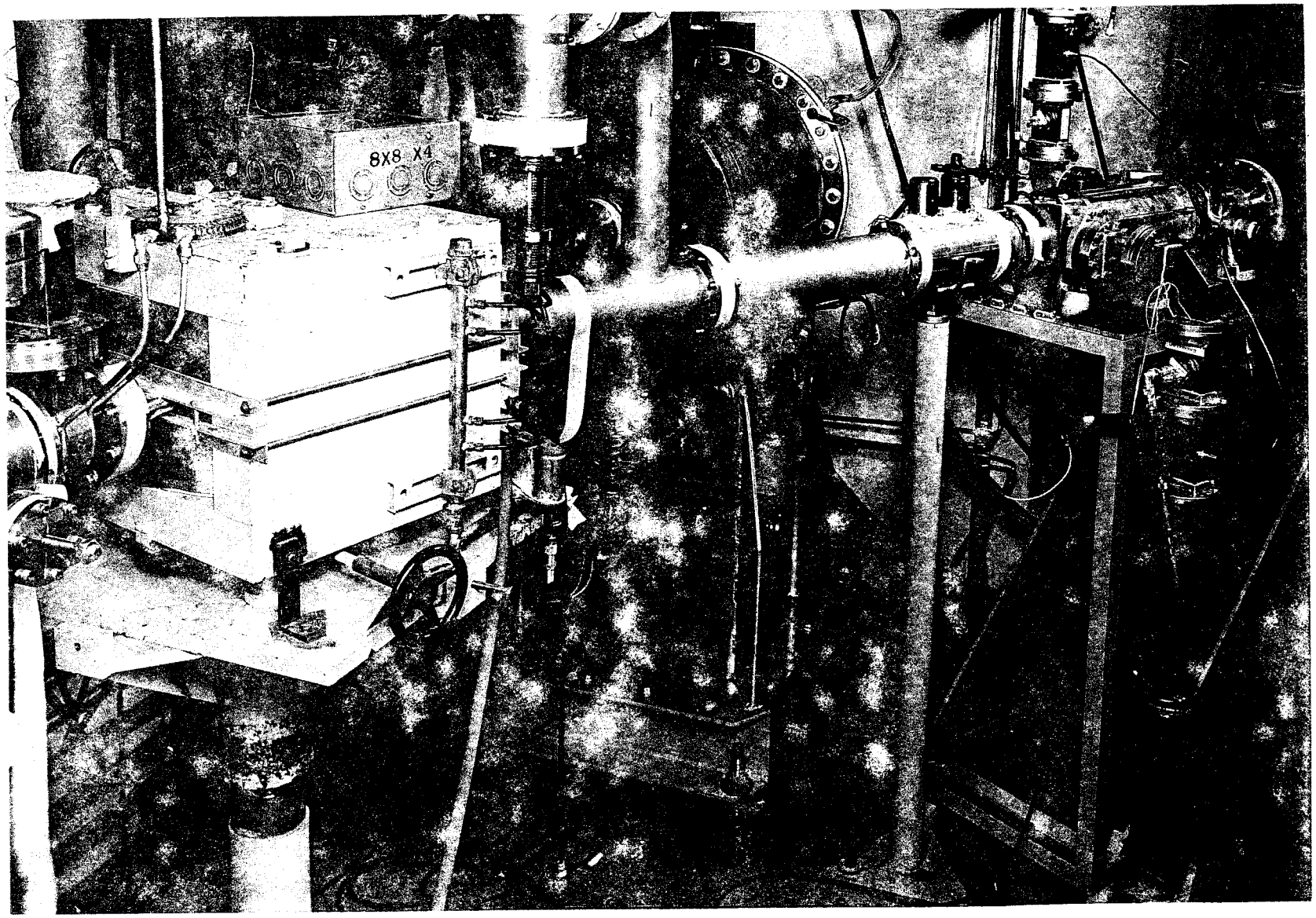

FIG. 15--Mark IV beam output showing momentum spectrometer, first drift tube, removable slits, rf separator model and second drift tube.

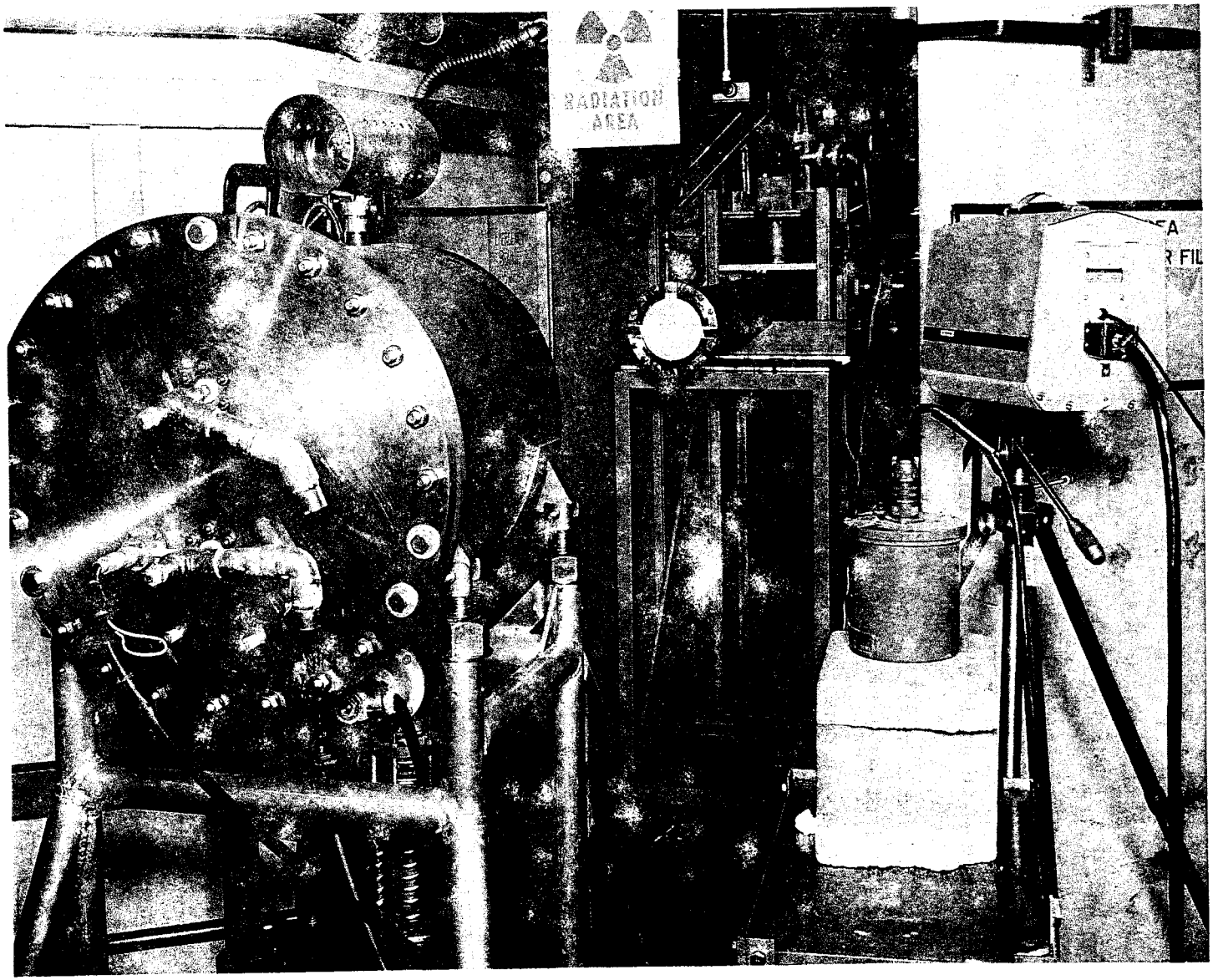

FIG. 16--Zinc sulphide target at output of rf separator drift tube with Faraday cup and television camera to monitor beam spot deflection.

The removable collimators at the end of each accelerator section and the width of the momentum slits made it possible to vary the beam cross section from 2.5 × 2.5 cm to 0.5 × 0.5 cm. By varying the strength of a steering dipole located at the beginning of the second accelerator section, it was possible to translate the beam relative to the axis of the separator by as much as ±1 cm in the vertical plane. The phase-bite of the electron beam was varied by making small changes in the operating frequency of the accelerator above 2857.3 Mc/sec. The entire system, from accelerator gun to ZnS screen, was evacuated to avoid multiple-scattering of the beam.

D. Experimental Results

1. Deflection Versus Phase

At a constant power level and beam momentum, the beam deflection was measured as a function of the relative phase of the fields in the separator with respect to the electron beam bunches. The results are shown in Fig. 17 where the abscissa is in units of linear displacement of the phase shifter. The data traces out a sine curve. This data was obtained for the separator without suppressor holes. In view of its similar behavior, it was not believed necessary to repeat this for the second model. For this measurement and for all subsequent ones the deflection was measured to an accuracy of ±1 mm (see Fig. 18).

2. Effect of Size of Phase Interval

By increasing the frequency above the operating frequency of the accelerator (2857.3 Mc/sec), the accelerated bunch width was changed. The effect that this has on the beam spot is shown in Fig. 19. The effect is most noticeable as one passes through the region of zero deflection, for it is in this region that the fields are changing most rapidly with phase.

3. Deflection Versus Power

By adjusting the attenuator to the separator, it was possible to vary the power into the separators without changing the energy of the electron beam. At all given power levels, the maximum obtainable deflection (as a function of phase) was measured. Figure 20 shows the maximum deflection as a function of the square root of the peak power in the structures. This is equal to the average of the peak deflecting field for negligible attenuation. An uncertainty of ±10 percent must be assigned to the power measurement, due primarily to the uncertainty in the input and output coupling ratios and the power meters. This uncertainty dominates the uncertainty in the value of the deflection. From

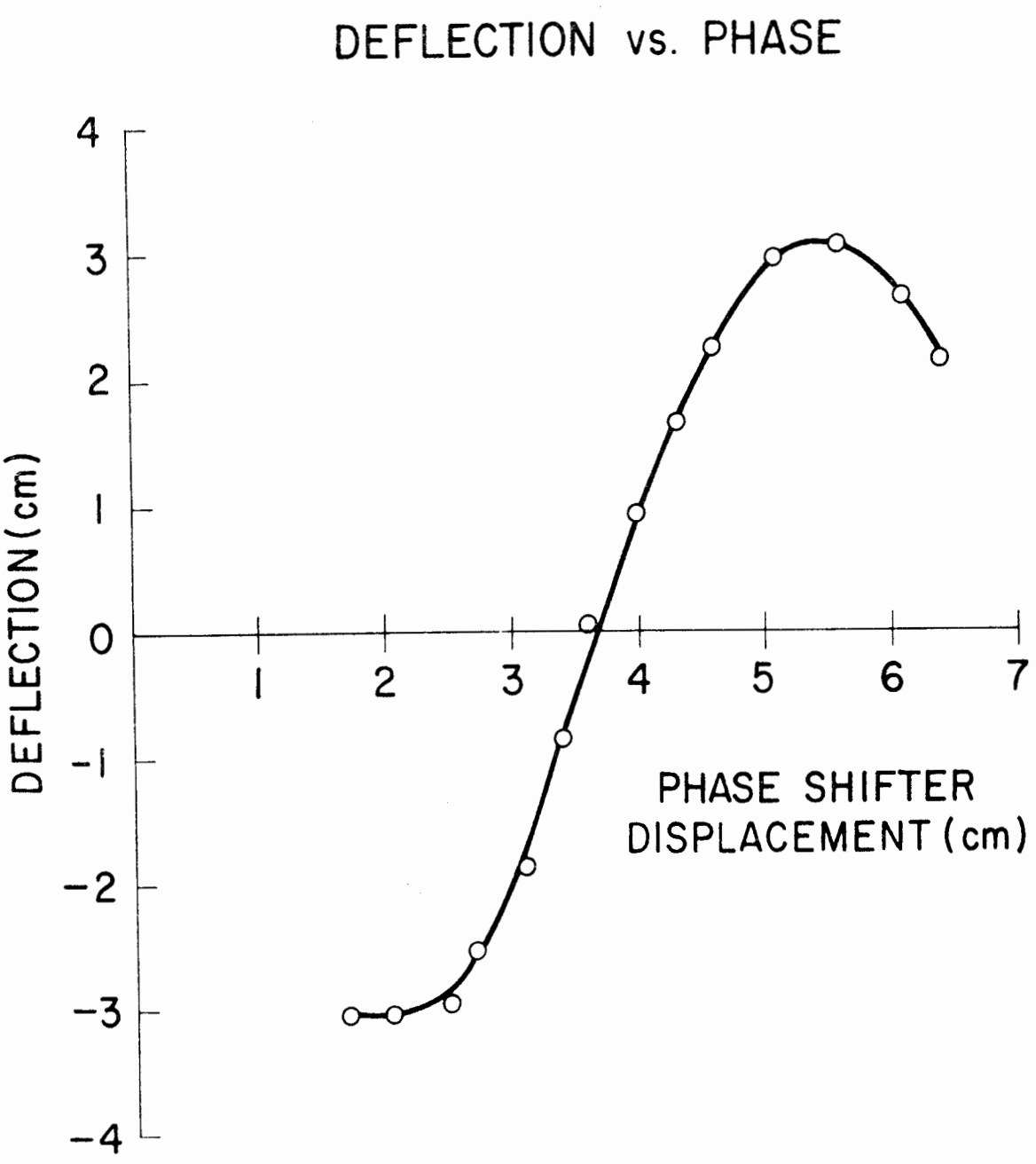

FIG. 17--Deflection versus phase.

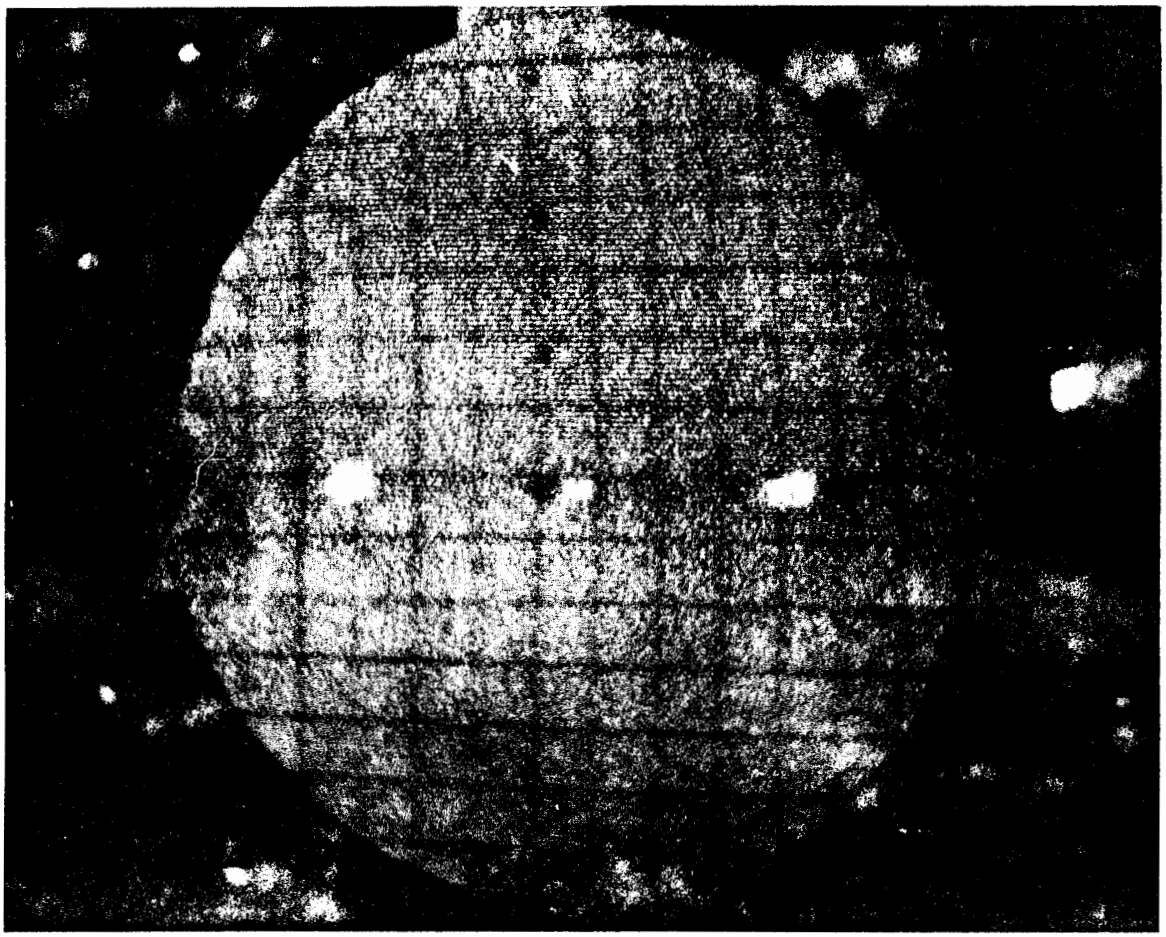

FIG. 18--Beam spots on ZnS screen for zero and extreme deflections (tight bunching).

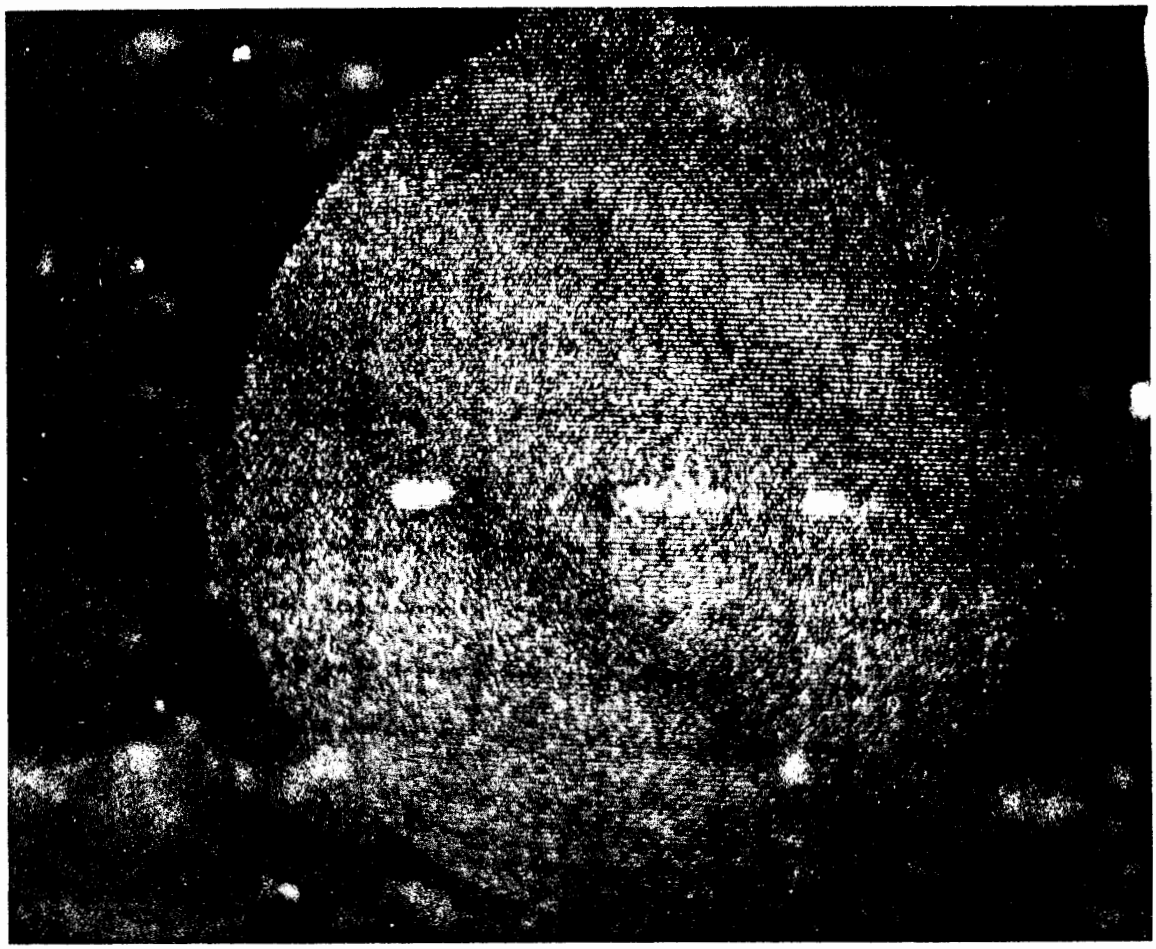

FIG. 19--Beam spots on ZnS screen for zero and extreme deflections (loose bunching).

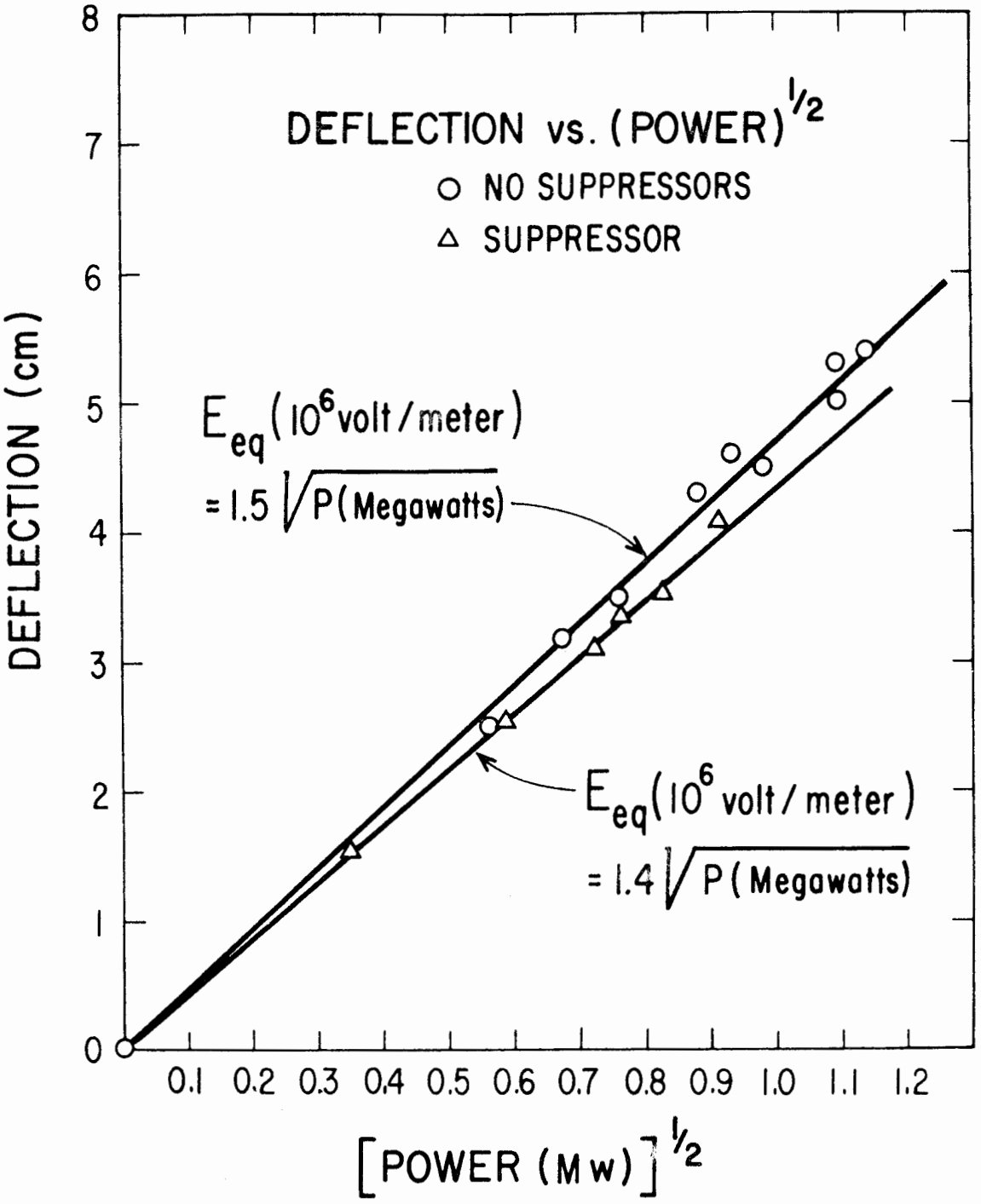

FIG. 20--Deflection versus $(\text{Power})^{\frac{1}{2}}$

the slope of the lines in Fig. 20 and a knowledge of the beam momentum and experimental geometry, the relation between the equivalent deflecting field strength and the power can be deduced:

$$E_{eq}(10^6 \text{ volt/meter}) = 1.5\sqrt{P(\text{Megawatts})} \tag{38}$$

for the structure with no suppressors and

$$E_{eq}(10^6 \text{ volt/meter}) = 1.4\sqrt{P(\text{Megawatts})} \tag{39}$$

for the structure with suppressors. The uncertainties are of the order of ± 5%.

4. Uniformity of Deflecting Field

By collimating the beam at the output of the first section and by activating the steering dipole at the beginning of the second section, a vertical transverse momentum was imparted to the electron beam. This resulted in a ±1.25 cm vertical excursion of the beam at the ZnS screen and, considering the geometry of the experimental arrangement, a ±1 cm excursion at the separator. Figure 21 shows that the maximum obtainable deflection of the beam is unchanged under these conditions. Both structures exhibited this behavior. It was impractical to explore the field uniformity near the disk edges.

V. CONCLUSIONS

A. Comparison of Theory and Experiment

H. Hahn has fed the dimensions of our structure into his computer program and calculated some of its properties. He obtained a relative group velocity of - 0.031, in good agreement with cold-test measurements (Section III). However, the calculation of $E_{eq} = 1.78\sqrt{P}$ is higher than the measured value (Section IV). In view of the complexity of the problem, the agreement between experiment and theory can be considered to be reasonably good. On the basis of the acceptances and separations obtained, it can be concluded that traveling-wave structures supporting this "TM_{11}-like" or HEM_{11} mode can be used as mass separators at multi-Bev energies.

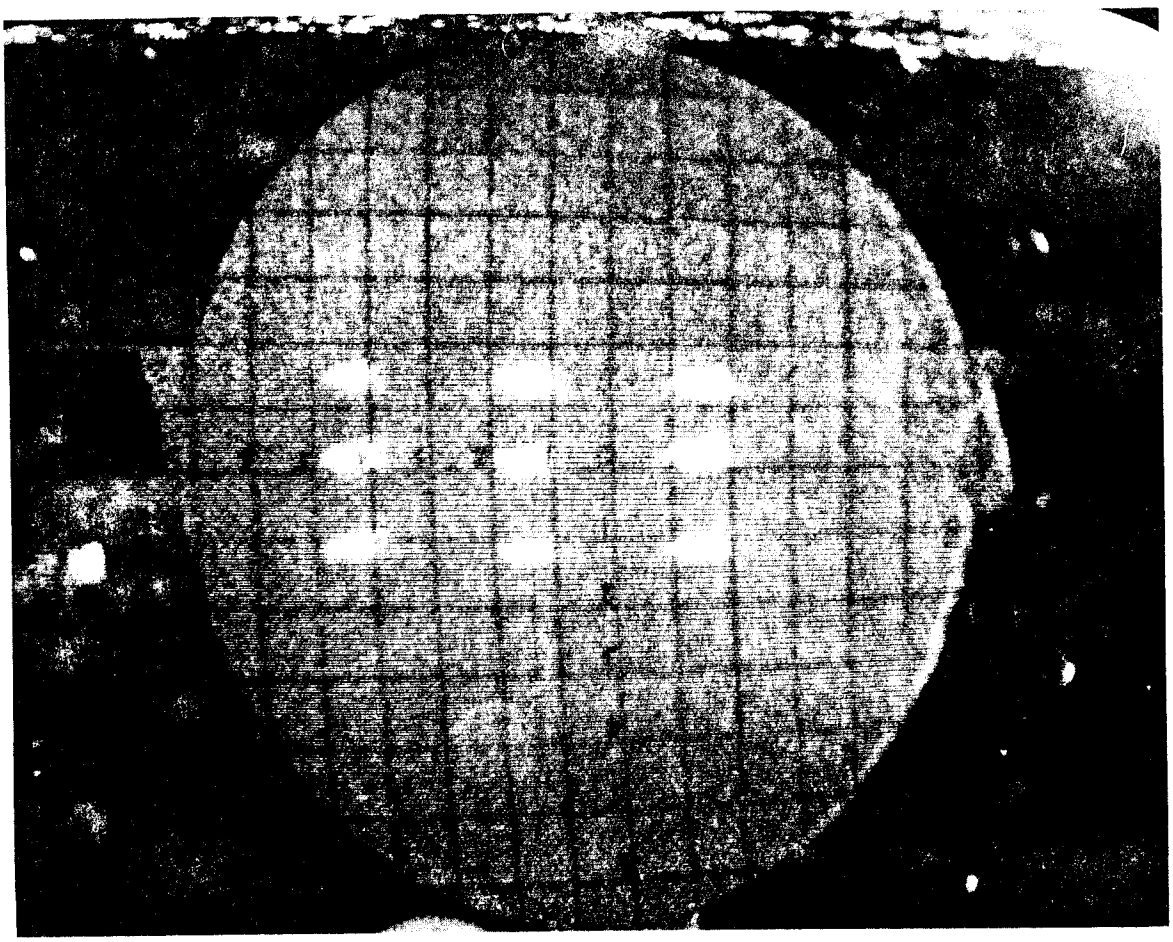

FIG. 21--Beam spots on ZnS screen for zero and extreme deflections at three different vertical positions. Notice aberration-free deflection.

B. A Remark on the Use of Resonant Cavities

As discussed in Section II.A, standing-wave structures suffer from a number of disadvantages. Assuming, however, that these disadvantages can be overcome, it is of interest to compare the effectiveness of Phillips-type cavity deflectors with traveling-wave structures of the type described in this paper. Phillips obtained an approximate deflecting field of $18\sqrt{P_{Mw}}$ Mv/meter for a one-half wavelength cavity. By optimizing the traveling-wave structure, it is believed that one can obtain at least $1.8\sqrt{P_{Mw}}$ Mv/meter. Hence, for a fixed amount of total power, it would take a minimum of 35 one-half wavelength cavities to obtain the same deflection as for a 3 meter traveling-wave structure. The advantage of a cavity array appears marginal, especially when one considers the complexity of the microwave circuitry and the phasing system involved to correctly feed these cavities.

C. Future Program at SLAC

The feasibility of traveling-wave separators has been demonstrated. Before adopting a final design for the two-mile accelerator, several parameters such as optimum group velocity, number of disks per wavelength, method of mode rotation suppression, resulting shunt impedance, etc., need to be investigated in greater detail. These activities will soon be undertaken at SLAC; the first step, presently underway, will be to build a model with a relative group velocity of - 0.007.

LIST OF REFERENCES

1951

1. W. Walkinshaw and J. S. Bell, AERE Report G/R 675 (1951).

1956

2. W.K.H. Panofsky, "A Mass Sensitive Deflector for High Energy Particles," HEPL-82 (Internal Memo), High Energy Physics Laboratory, Stanford University, Stanford, California (May 1956).
3. W.K.H. Panofsky and W. Wenzel, "Some Considerations Concerning the Transverse Deflection of Charged Particles in Radio-Frequency Fields," Rev. Sci. Instr. 27, 967 (1956).

1957

4. R. B. Neal, "Design of Linear Electron Accelerators With Beam Loading," Microwave Laboratory Report No. 379, Hansen Laboratory of Physics, Stanford University, Stanford, California (March 1957).
5. E. L. Ginzton, Microwave Measurements, McGraw-Hill Book Company (1957).

1958

6. J. P. Blewett, "A New Type of Resonant Cavity for Deflection of Particle Beams," Internal Report JPB-9, Brookhaven National Laboratory (March 1958).
7. H. G. Hereward, "Particle Separation Using Internal Bunching," CERN PS Int. Th 58-8, CERN, Geneva, Switzerland (December 1958).
8. V. I. Veksler, "Starting Up of a 10 BeV Synchrophasotron and First Results of Physical Research," Proceedings Second U.N. Conference Peaceful Uses of Atomic Energy, P/2229, v. 30, 1958; p. 3.

1959

9. J. P. Blewett,"A Radio-Frequency Mass Separator for Complete Separation of High-Energy Particle Beams," Proceedings of the International Conference on High-Energy Accelerators, CERN, Geneva, Switzerland, 1959; p. 422.
10. W.K.H. Panofsky, "Remarks on High Energy Microwave Separators," CERN, Geneva, Switzerland, 1959 (internal memorandum).
11. "Linear Electron Accelerator Studies, Status Report 1 October to 31 December 1958," Microwave Laboratory Report No. 581, Stanford University, Stanford, California (1959).

1960

12. R. Belbéoch, "Déflexion de particules relativistes par des champs electromagnétiques," Report LAL 11, Orsay, France (October 1960).

13. M. Geiger, "Particle Separation by Means of a Chain of RF Deflection Cavities," Part I & II, CERN PS/Int. AR/PSep. 60-4, CERN, Geneva, Switzerland.

14. M. Geiger, "Some Considerations on Particle Separation by Means of RF Deflection Using Cavities," CERN Report No. AR/60-13, CERN, Geneva, Switzerland.

15. P. Lapostolle, "Sur la déflection d'une particule rapide par un champ électromagnétique," CERN PS/Int. AR/PSep. 60-2, CERN, Geneva, Switzerland.

16. P. Lapostolle, "Focalisation alternée dans un séparateur haute fréquence; séparateurs paramétriques," CERN PS/Int. AR/PSep. 60-5, CERN, Geneva, Switzerland.

17. P. Lapostolle, "Quelques relations approximatives concernant la séparation de particules de même quantité de mouvement mais de masse différente au moyen de champs de haute fréquence," CERN PS/Int. AR/60-15, CERN, Geneva, Switzerland.

18. B. W. Montague, "RF Travelling Wave Particle Separators; a Matrix Formalism and General Phase Space Properties," CERN PS/Int. AR/PSep. 60-1, CERN, Geneva, Switzerland.

19. P. R. Phillips, "The Separation of High-Energy Particle Beams by Microwave Techniques," Ph.D. Thesis, Stanford University, Department of Physics, (November 1960).

1961

20. K. L. Brown et al., "Linear Electron Accelerator Progress at Stanford University," Proc. International Conf. High Energy Accelerators, Brookhaven National Laboratory, New York; p. 79 (1961).

21. M. C. Crowley-Milling et al., "Pulse Shortening in Electron Linear Accelerators," Nature, Vol. 191, p. 483 (1961).

22. M. M. Geiger, P. Lapostolle and B. Montague, "La séparation des particules au moyen de champs hf," CERN Report No. 61-26, CERN, Geneva, Switzerland.

23. B. W. Montague, Personal Communication with Dr. A. Robertson, July 18, 1961. BWM/kt.

24. W. Schnell, "Discussion of a Radio Frequency Particle Separator for the CERN Proton Synchrotron," CERN Report No. 61-5, CERN, Geneva, Switzerland.

1962

25. J. W. Bittner, Internal Report BNL-AGS, JWB-1 (1962).

26. E. L. Chu, "Separation of High Energy Charged Particles by RF Deflection," Technical Note TN-62-12, Stanford Linear Accelerator Center, Stanford University, Stanford, California (March 1962).

27. E. L. Chu, "Subharmonic RF Separators," Technical Note TN-62-14, Stanford Linear Accelerator Center, Stanford University, Stanford, California (March 1962).

28. A. L. Eldredge, G. A. Loew and R. B. Neal, "Design and Fabrication of the Accelerating Structure for the Stanford Two-Mile Accelerator," SLAC Report No. 7, Stanford Linear Accelerator Center, Stanford University, Stanford, California (1962).

29. "Future Program for the CERN PS and Brookhaven AGS," Minutes of a Meeting held September 10-14, 1962 at Brookhaven National Laboratory.

30. Yves Garault, "Electromagnetic Waves of the E. H. Type in a Circular Waveguide with Metallic Irises," Comptes Rendus, Paris, Vol. 255, p. 2920 (1962).

31. Yves Garault, "Propriétés générales d'un type d'ondes utilisables dans les accélérateurs pour les déflecteurs h.f. de particules rapides," GT/62-1, Orsay, France (1962).

32. Yves Garault, "Ondes EH du guide cylindrique circulaire chargé par des iris métalliques," Gt/62-2, Orsay, France (1962).

33. Yves Garault, "Étude des lignes de force du champ électromagnétique du mode EH_{11} déflecteur du guide à iris," Gt/62-3, Orsay, France (1962).

34. H. Hahn, "The Deflecting Mode in the Circular Iris-Loaded Waveguide of a RF Particle Separator," Internal Report BNL-AGS, HH-5 (1962).

35. H. Hahn, "Longitudinal Electromagnetic Modes in Circular Cylinder Coordinates," Internal Report, Brookhaven National Laboratory HH-4 (May 1962).

36. H. Hahn, "The Brookhaven RF Particle Separator," Minutes CERN-BNL Meeting, Brookhaven National Laboratory, New York; p. 103 (1962).

37. H. G. Hereward, "Radio Frequency Beam Separators at CERN," Minutes CERN-BNL Meeting, Brookhaven National Laboratory, New York; p. 94 (1962).

38. International Conference on Instrumentation for High Energy Physics, CERN, Geneva, Switzerland (July 1962).

39. E. Keil, B. W. Montague, W. W. Neale, Int. Report CERN/TC/NBC 62-2.

40. E. Keil and B. W. Montague, "Some Secondary Beams From Internal Targets in a PS Magnet Unit," CERN/AR/PSep. 62-2, CERN, Geneva, Switzerland (internal memorandum).

41. E. Keil, "Parameters for RF Separation of π and K at 100 Gev/c Design Momentum," CERN AR/Int. PSep/62-3, October 1962.

42. J. E. Leiss and R. A. Schrack, "Transient and Beam Loading Phenomena in Linear Electron Accelerators," Internal Report, National Bureau of Standards; p. 47 (1962).

43. W. Schnell, "Discussion of a Radio Frequency Particle Separator for the CERN Synchrotron," CERN Report No. 61-5, CERN, Geneva, Switzerland (1962).

44. "Two-Mile Accelerator Project, Quarterly Status Report, 1 July to 30 September 1962," SLAC Report No. 8, Stanford Linear Accelerator Center, Stanford University, Stanford, California (1962).

1963

45. H. Hahn, "Space Harmonic Analysis of the $\pi/2$ Deflecting Mode: The Maximum Deflection," BNL-AGS Report HH-6, Brookhaven National Laboratory, New York (April 1963).

46. H. Hahn and H. J. Halama, "Mode Identification in the Iris-Loaded Waveguide of an RF Particle Separator," AGS Internal Report HH/HJH-2, Brookhaven National Laboratory, New York (January 1963).

47. E. Keil, "Tolerances on RF Separator Parameters," CERN AR/Int. PSep/63-3.

48. J. Sandweiss, "RF Separated Beams for the 80-Inch Bubble Chamber," Report No. H-H-13 (BC), Brookhaven National Laboratory, New York (April 1963).

49. "Two-Mile Accelerator Project, Quarterly Status Report, 1 October to 30 December 1962," SLAC Report No. 10, Stanford Linear Accelerator Center, Stanford University, Stanford, California (March 1963).

50. "Two-Mile Accelerator Project, Quarterly Status Report, 1 January to 31 March," SLAC Report No. 16, Stanford Linear Accelerator Center, Stanford University, Stanford, California (May 1963).